Analysis of New Multi Cellular Vortex Model

Israt Jahan Eshita

A Thesis

In the Department

of

Mechanical Engineering

Presented in Partial Fulfillment of the Requirements

For the Degree of Master of Applied Science at

Concordia University

Montréal, Québec, Canada

July 2014

CONCORDIA UNIVERSITY

School of Graduate Studies

This is to certify that the thesis prepared

By: Israt Jahan Eshita I.D. 9806946

Entitled: Analysis of New Multi Cellular Vortex Model

and submitted in partial fulfillment of the requirements for the degree of

Master of Applied Science in Mechanical Engineering

complies with the regulations of the University and meets the accepted standards with respect to originality and quality.

Signed by the final examining committee:

Dr. M. Kazemi Zanjani Chair

Dr. Henry Hong Examiner

Dr. Andreas K. Athienitis Examiner

Dr. Georgios Vatistas Supervisor

Approved by: Chair of Department or Graduate Program Director

Dean of Faculty

Date August 14th, 2014

ABSTRACT

Analysis of New Multi Cellular Vortex Model

Israt Jahan Eshita

A complete theoretical description of multi-celled vortices is complex. Nevertheless, a simplified approach like the one presented in this thesis can provide the most fundamental characteristics satisfactorily.

In this model all velocity distributions are bounded. The solution is obtained using MATLAB and Maple 14 code. The main goal is to develop a numerical technique that will provide good fits to a variety of actual vortices of different types.

The simulated results correlate well actual data of some naturally and experimentally occurring vortices. Two-celled vortices developed in the intakes of gas turbine engines operating near the ground, wing-tips, tornadoes and vortices generated under a liquid-air interfacial wave by wind action are examined here.

The correlations provided in this thesis are biased towards two-cell vortices because a fair number of actual data for the velocity are readily available in the scientific literature. In addition, a simulated four-cell vortex model also described.

Acknowledgements

I would like to express my sincere gratitude to my supervisor Dr. Georgios H. Vatistas for his guidance, advice and financial support to finish this dissertation. He is more than a supervisor to me.

I am really grateful to him for initiating this project and always promoting me to think further. He gave me the opportunity to work under his supervision in his research group. He urged me to work in his group by constantly thinking and asking questions to myself at every step of my practical and writing work, which helped me to always think creatively and rationally.

I would also like to thank my examiners for managing to read my manuscript and give their valuable opinions and advices. I would like to thank my lab mates for their encouragement, help and support. They are really helpful and cooperative. I have good time with them through the two years.

Very special thanks to my husband for his spontaneous cooperation, friendship, sanity, great times and love. It is really tough for me to live without my parents and family for a long period of time. That time my husband is always beside me, help me with the moral support, and encourage me at every step of my life.

I would like to express my deepest gratitude to my mother and father for their prayers, well wishes love, blessings and support throughout my life. No words

could properly thank the wonderful parents and two younger brothers, who are always believing in me and encouraging me. I am really thankful for their continued financial and emotional support.

Last but not least, I am extremely grateful to Almighty for his blessing and kindness upon me. The almighty merciful, kindly gives me the strength and ability to complete my thesis.

Table of Contents

List of Figures

List of Tables

NOMENCLATURE

Listed below are the main symbols, which are used in this thesis. Note that more than one meaning maybe assigned to a symbol. Other symbols are described internally.

a = constant

C = arbitrary constant

f = general function

m,i = constant exponents

n = constant exponents

N = number of cells

P = static pressure, Pa

Re = the vortex Reynold's number

r,z = radial and axial cylindrical coordinates

s, t = dummy variables.

$\boldsymbol{V}$ = velocity

x,y,z = Cartesian coordinates.

V_θ = Non dimensional tangential velocity.

V_r = Non dimensional radial velocity.

V_z = Non dimensional axial velocity.

$r=r^*/r_c^*$ = Non dimensional radius.

r_c^* = Dimensional core radius

x,y = Cartesian coordinates

Greek Symbols

α = arbitrary constant

β = scaling constant

Γ^* = circulation, m^2/s

$\Delta\Pi$ = normalized pressure

κ_1 = constant scaling parameters

κ_2 = scaling parameters

λ = positive smallest root

η = scaling constant

η_1 = model constant

η_2 = model constant

ν^* = kinematic viscosity, m^2/s

ρ^* = density, kg/m^3

Ω = vorticity

Ω_z = non dimensional vorticity

Subscripts

c = quantity at the vortex core

r, θ, z = radial, tangential and axial component

0 = quantity at the vortex center

∞ = dimensional quantity

Superscript

* = dimensional quantity

Chapter 1 Introduction

1.1 The Problem

Vortices are known to play a vital part in transporting mass momentum and energy in many areas of science and technology. The last fact motivated researchers to study their most fundamental characteristics since the 19th century. For one-cell vortices, where the radial flow converges from far field and then rises upwards near the axis of rotation, there are several well-known models in existence.

This is not however the case for the multi-cellular (*N*-cells) type. The so-called two-celled vortex consists of two kinds of flow structures that take place in the meridional (*r*-*z*) plane. There is a region near the axis of rotation where the fluid drops from above and then diverges radially outwards near the vortex base. At a specific location, it meets the converging flow arriving from the outer periphery whereby both meet and deflect upwards (see Fig. 2.3.2). Two-celled vortices are also characterized by a very modest (if not zero) rotation near the origin. It was long known that at least one third (if not more) of the tropical and localized severe storms could mature from the severe one-cell type to devastating two-cell vortices [1]. This kind of whirls are not however exclusive to atmospheric sciences. Mechanically produced vortices could also display the two-cell fundamental characteristics [3].

Until the late 19 hundreds, the now famed Sullivan's vortex was the only simple model that could predict the previously mentioned downdraft/updraft combination of the two-celled vortices. In 1998 Vatistas et al published on a novel model that was able to simulate both single and double-celled vortices while all velocity components remained bounded in the radial direction. The most popular member of the single-cell group is the n = 2 [4]. Its mathematical simplicity has made it particularly valuable in numerous studies that range from helicopter blade aerodynamics to dust devils in Mars.

In this thesis, the original two-cell vortex is enlarged to include a wide range of multi-celled vortices of relevance to natural and technological whirls [4]. Our analysis focuses on model correlations with actual observations of velocity and static pressure.

1.2 Previous Work

As mentioned earlier, most of the approximate models, which have been developed in the past, pertain to single cell vortices. Rankine proposed the simplest of these 156 years ago. His formulation, still in use, assumes a linear tangential velocity distribution inside the core region $0 \leq r^* \leq r_c{}^*$(where r^* is the radial coordinate, $r_c{}^*$ is the radius where the tangential velocity attains its maximum value), and a hyperbolic variation in the interval $r_c{}^* \leq r^* \leq \infty$ [5]. This velocity distribution however, generates an unrealistic sharp pinnacle for the velocity at the core ($r_c{}^*$),

and renders the vorticity discontinuous at the point of transition from forced to free vortex modes. Also, the nature of this formulation requires that both the radial and axial-velocity components to be zero. In spite of these weaknesses, the static pressure approximates reality quite well, which suggests further that the velocity deviations from the experimental values near the core do not influence the pressure profile significantly.

The Kaufmann-Scully (Kaufmann (1962)-Scully (1975) [6]), popularly known as Scully's vortex, is an empirical vortex model where the tangential velocity encompasses the smoothing effects of viscosity close to the core radius [6,7]. Although it assumes non-zero radial and axial velocity components this model nonetheless underestimates most of the measured values of tangential velocity near the core radius.

Burgers in 1948 proposed another single celled vortex model, which produced an improvement between the predicted and observed values of tangential velocity near the core [7]. However, it assumes a linear profile for the radial-velocity, and a constant axial-velocity, making the model to be non-bounded and therefore not suitable for further treatment for unconfined vortices, such as for example compressible two celled vortices.

In 1959 based on Burgers' work, Sullivan proposed a double cellular structure, where the radial and axial velocity components reverse their directions near center

of vortex thus producing a central recirculation zone [8]. Being a model that was based on Burgers's, this too produces unbounded radial velocity.

The development of velocity and vorticity is not the same for all vortices. A vortex such as strong tornadoes may develop zero velocity and vorticity near the origin, known as the "vortex eye". None of the classical single- or double-celled vortex models predict convincingly this property.

In 1991 Vatistas et al. proposed a new vortex formulation, which is now familiar as the *n*-vortex model [9], capable in producing a family of bounded velocity distributions. Depending upon the value of the exponent *n*, one can simulate the tangential velocity distributions of the classical formulations such as Rankine to Kaufmann-Scully, and also approximates closely Burgers's. The tangential, radial and axial velocities are bounded in the interval [0, ∞]. The axial velocity ranges from a pure jet-like to profile with a 100% deficit at the central axis to jet-like [4]. Percentages of vorticity more or equal to 50% existing inside the core makes them concentrated. This approach made further developments of unconfined vortices possible.

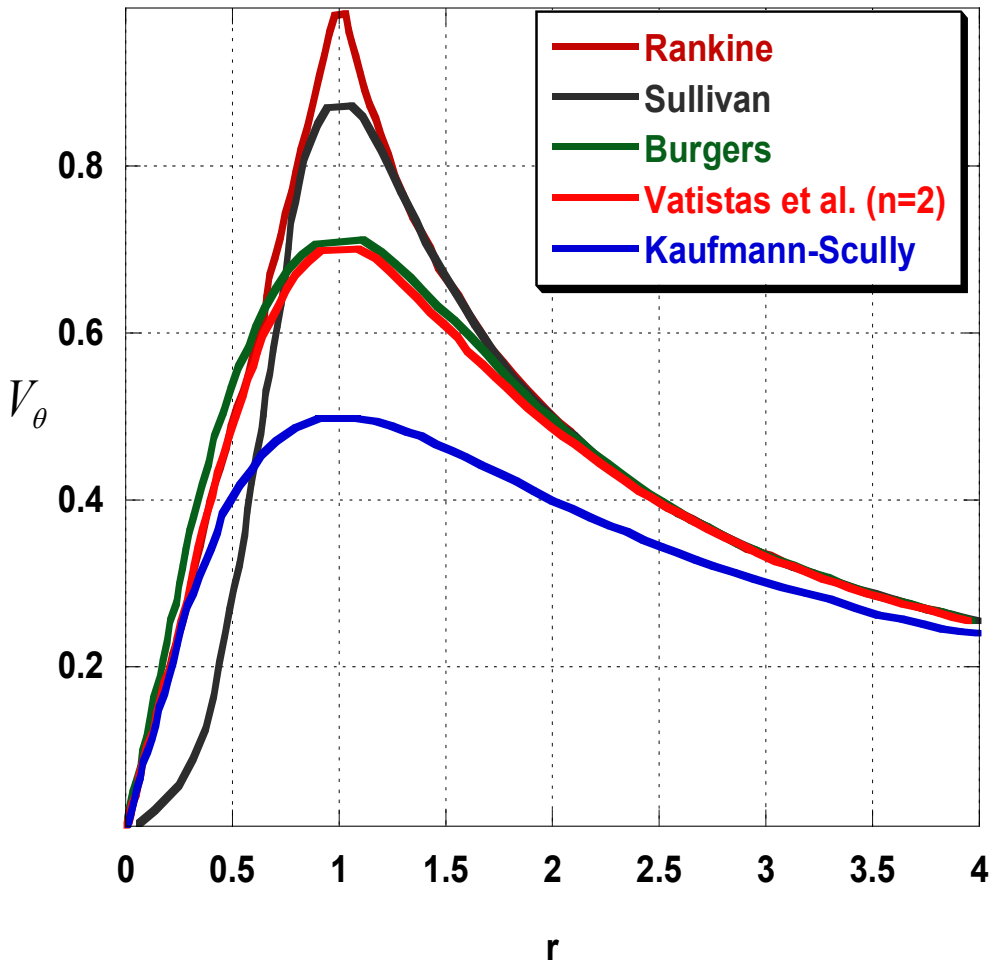

Figure 1.2.1 Tangential velocity profiles for different past vortex models (V_θ= Non dimensional tangential velocity).

From Fig. 1.2.1 we observe that in Rankine's vortex the tangential velocity distribution is linear inside the core (radius of maximum tangential velocity, where r =1) and hyperbolic outside of core [5]. The velocity changeover from linear to hyperbolic modes creates a sharp pinnacle at the core radius. The expected smoothing effect of viscosity in the last region is present in Sullivan's, Burgers', Vatistas' et al (n =2) and Kaufmann-Scully (or n = 1) models.

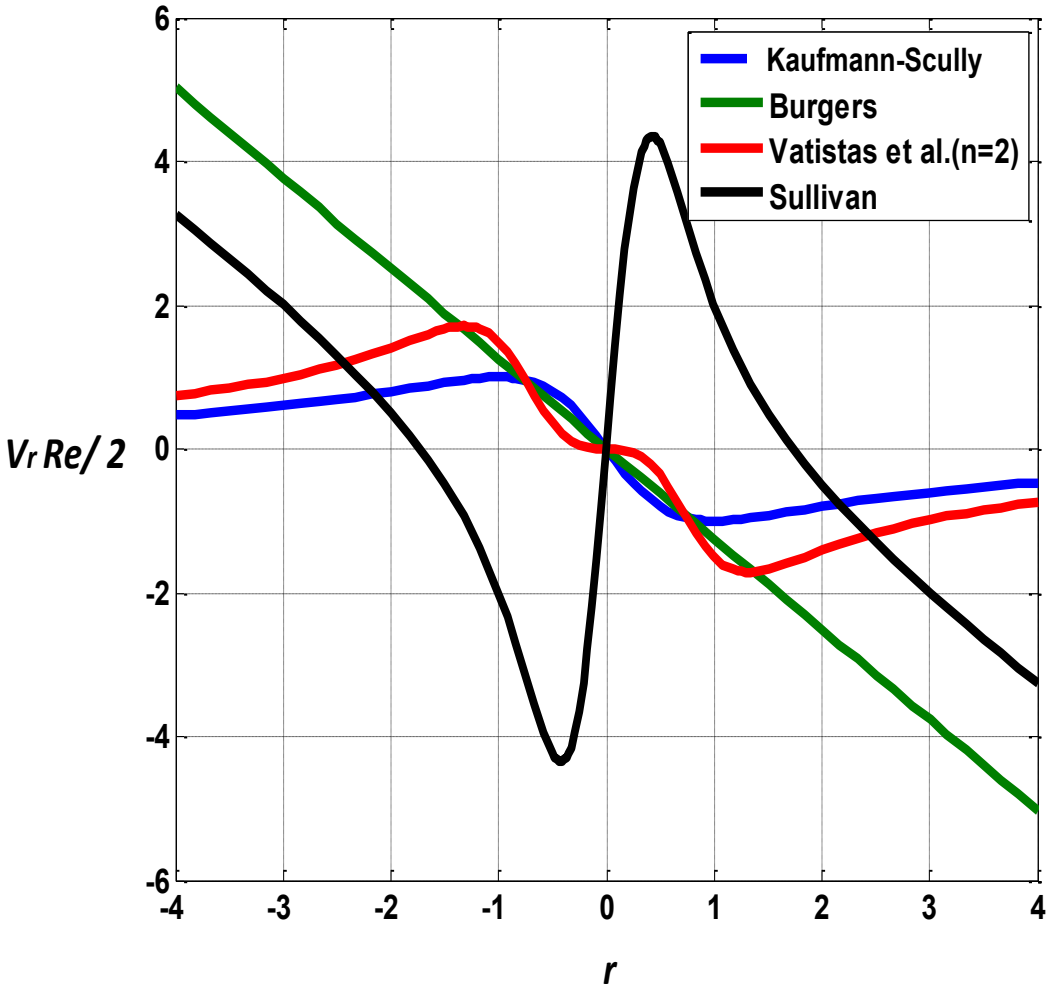

Figure 1.2.2 Radial velocity profiles for different past vortex models (where, V_r = Non dimensional radial velocity).

The radial velocity of Sullivan, Burgers, Vatistas et al (n =2), Kaufmann-Scully models are shown in the Fig. 1.2.2. This velocity component is zero in Rankine's and linear in Burgers's vortices.

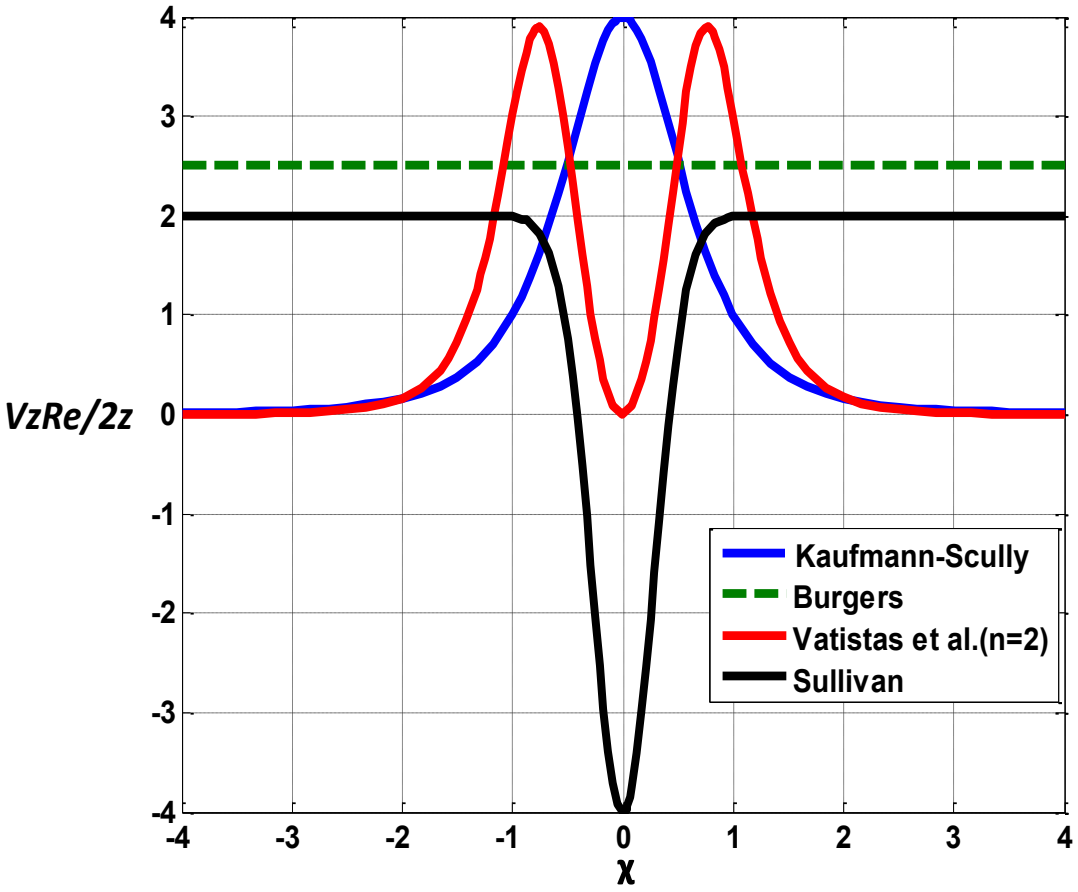

Figure 1.2.3 Axial velocity profiles for different past vortex models, (where, V_z = Non dimensional axial velocity).

Since the radial velocity in Sullivan's and Burgers's formulations grows continually with the radius makes them unbounded, and thus unsuitable without any other drastic simplification. From Fig. 1.2.3 the axial velocity of Sullivan, Burgers, Vatistas et al (n =2), Kaufmann-Scully models are shown. The axial velocity component is zero in Rankine's and constant in Burgers's vortex models.

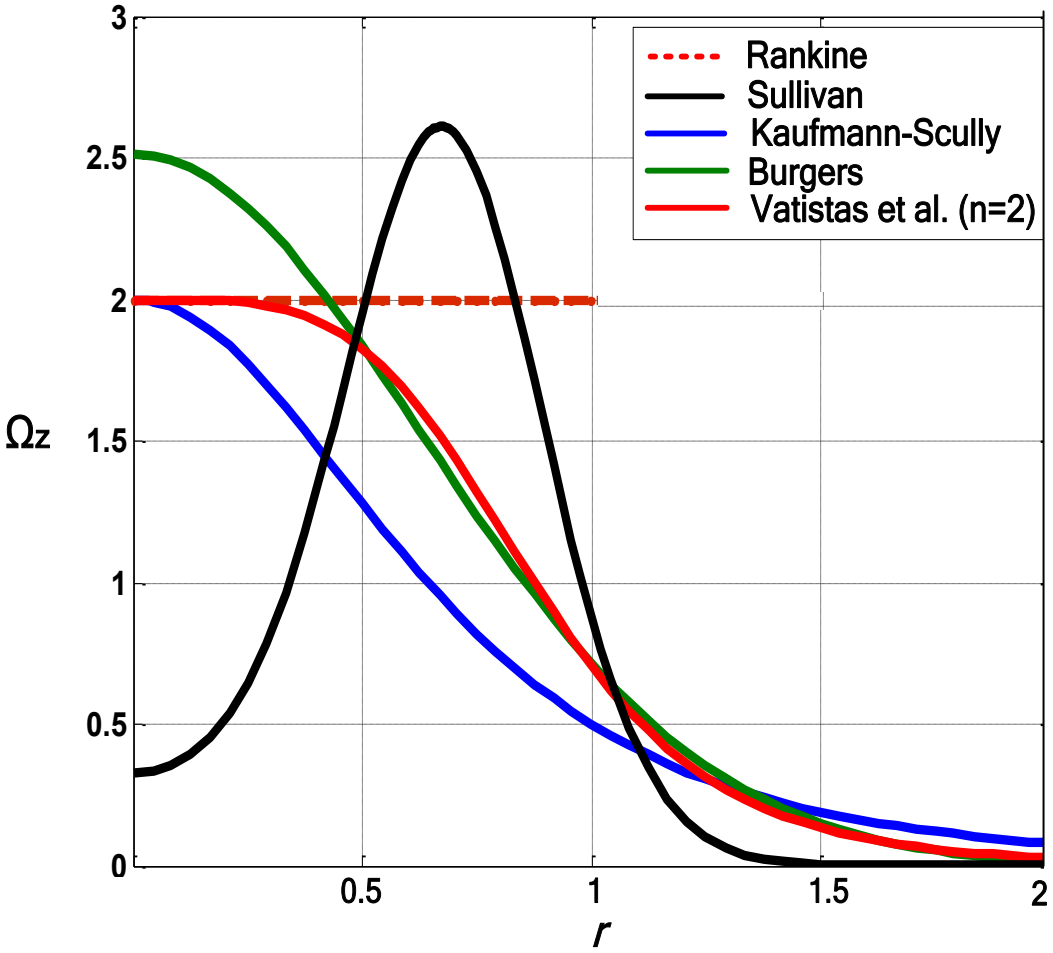

Figure 1.2.4 Vorticity of profiles for different past vortex models (Where, Ω_z = Non dimensional vorticity)

The corresponding vorticity distributions for all the previous models are shown in Fig. 1.2.4. The sudden changeover of the tangential velocity in Rankine's vortex renders the associated vorticity to be discontinuous at the point of transition.

Table 1.2.1 Percentage of vorticity inside the core for different vortex models [4].

Vortex model	**%of vorticity**
Rankine vortex	100
Kaufmann-Scully	50
Burgers	71.05
Sullivan	88.3
Vatistas et al. model (n= 2)	70.70

The percentage of vorticity existing within the core for the different vortex models is given Table 1.2.1. Because the vortex core contains most of the vorticity, makes these vortices concentrated.

Table 1.2.2 Velocity formulas for different vortex models [4].

Vortex model	V_θ	V_r	V_z / z
Rankine	r, for r in [0, 1] $1/r$, for every r in $[1, \infty)$	0	0
Kaufmann -Scully	$\frac{r}{1+r^2}$	$-\frac{4}{Re}\frac{r}{1+r^2}$	$\frac{8}{Re}\frac{r}{(1+r^2)^2}$
Burgers	$\frac{1}{r}\left[1-\exp(-\eta_1 r^2)\right]$	$-\frac{2\eta_1}{Re}r$	$\frac{4\eta_1}{Re}$
Vastistas et al.	$\frac{r}{(1+r^{2n_1})^{1/n_1}}$	$-\frac{2(n_1+1)}{Re}\frac{r^{2n_1-1}}{(1+r^{2n_1})}$	$\frac{4n_1(n_1+1)}{Re}\frac{r^2(n_1-1)}{(1+r^{2n_1})^2}$
Sullivan	$\frac{1}{r}\frac{H(\eta_2 r^2)}{\lim_{r\to\infty} H(\eta_2 r^2)}$	$\frac{2}{Re}\left\{-r+\frac{3}{r}\left[1-\exp(-\eta_2 r^2)\right]\right\}$	$\frac{4}{Re}\left[1-3\exp(-\eta_2 r^2)\right]$

$\eta_1 = 1.256,\ \eta_2 = 6.238$

Table 1.2.2 summarizes the formulae for the velocity components associated with all the previous vortex models.

1.3 The Contribution

The original single-cell $n = 2$ vortex model, presented in Vatistas et al. [9] correlates well many vortices. Several vortices however, are also known to be of the multi-celled type. In order to represent the last characteristic, $n = 2$ vortex model was extended to include this property [4]. The present study moves one step ahead extending the mathematical formulation of Vatistas [4] to describe multi-celled vortices. The solution is obtained using the MATLAB and Maple 14 software.

Although, it is well known that, some vortices like mature hurricanes develop more than two cells, there are no however detailed velocity data to perform reliable correlations. Due to the last mentioned reason, the correlations in this thesis are biased towards two-cell vortices because a fair number of actual data for the velocity exist in the scientific literature.

The new methodology is also shown to fairly correlate the observations of naturally occurring and industrial vortices. In the process a more general form of Sullivan's double-cell vortex was analyzed [8].

Chapter 2 Mathematical Modeling

2.1 The Theoretical Frame of the Problem

We consider here a steady, axisymmetric, incompressible vortex. The usual assumption that considers V_r and V_θ to be functions of the radius (r) only is implemented. Furthermore, the radial (V_r) and axial (V_z) velocity components in strong vortices are substantially weaker than the tangential (V_θ),

$$V_r = \frac{V_r^*}{V_c^*} \text{ and } V_Z = \frac{V_z^*}{V_c^*} \text{ are } \quad << 1$$

Where,

$$V_c^* = \frac{\Gamma_\infty^*}{2\pi r_c^*}$$

and Γ_∞^* is the vortex circulation.

The mathematical modeling of the problem starts from continuity and the Navier-stokes equations. According to the previous assumptions, the equations of motion in cylindrical coordinates are as follows:

Continuity:

$$\frac{\partial V_r}{\partial r} + \frac{V_r}{r} + \frac{\partial V_z}{\partial z} = 0$$
$$\delta \quad \delta \quad \delta \qquad \text{(2.1.1 a)}$$

All the terms in the continuity equation have same order of magnitude (where δ represents a very small number with order ranging10^{-5} to 10^{-7}, see Table 2.1.1). Therefore, this equation remains as is**.**

Radial, *r*- momentum:

$$V_r \frac{\partial V_r}{\partial r} + V_z \frac{\partial V_r}{\partial z} - \frac{V_\theta^2}{r} = -\frac{\partial \Delta\Pi}{\partial r} + \frac{1}{\mathrm{Re}}\left(\frac{\partial^2 V_r}{\partial r^2} + \frac{1}{r}\frac{\partial V_r}{\partial r} - \frac{V_r}{r^2} + \frac{\partial^2 V_r}{\partial z^2} \right)$$
$$\delta \quad \delta \qquad \delta \quad \delta \quad 1 \qquad\qquad \delta \quad \delta \qquad \delta \quad \delta \quad \delta \qquad \text{(2.1.1 b)}$$

The radial momentum equation contains one term having order of magnitude 1.

Axial, *z* - momentum:

$$V_r \frac{\partial V_Z}{\partial r} + V_z \frac{\partial V_Z}{\partial z} = -\frac{\partial \Delta\Pi}{\partial z} + \frac{1}{\mathrm{Re}}\left(\frac{\partial^2 V_Z}{\partial r^2} + \frac{1}{r} \frac{\partial V_Z}{\partial r} + \frac{\partial^2 V_Z}{\partial z^2} \right)$$

(2.1.1 c)

Tangential, θ-momentum:

$$V_r \frac{\partial V_\theta}{\partial r} + \frac{V_r V_\theta}{r} = \frac{1}{\mathrm{Re}}\left(\frac{\partial^2 V_\theta}{\partial r^2} + \frac{1}{r} \frac{\partial V_\theta}{\partial r} - \frac{V_\theta}{r^2} \right)$$

(2.1.1 d)

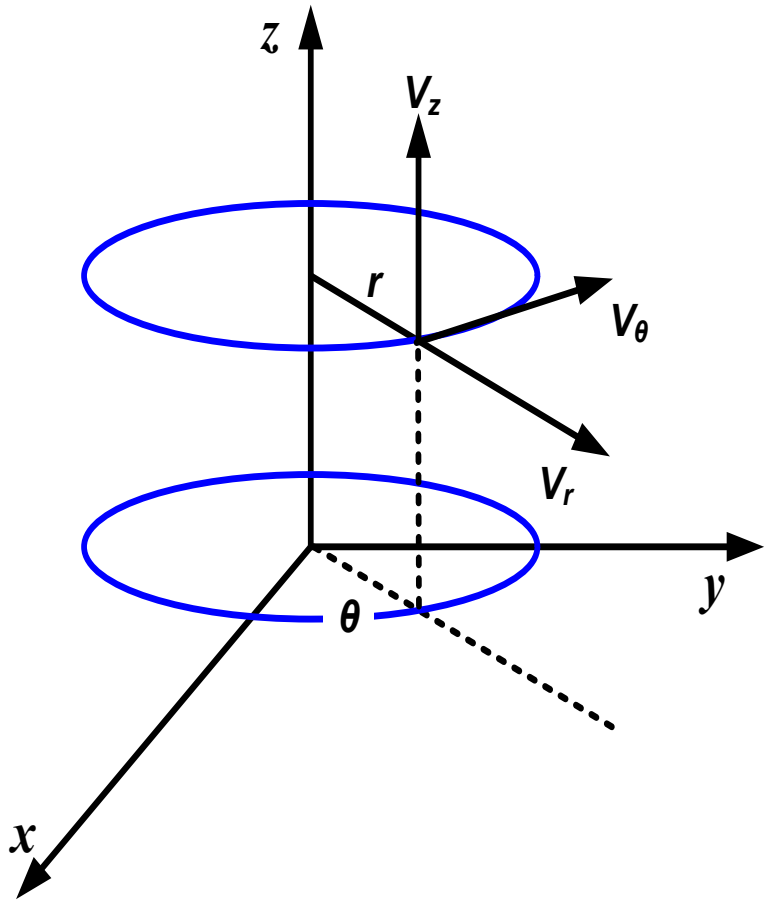

Figure 2.1.1 Coordinate system for a multi-cell vortex.

Table 2.1.1 Representative order of magnitude of δ for various vortices.

Vortex type	r_c^* (m)	$V_{\theta max}{}^*$ (m/s)	Re	δ
Tornadoes	10.0	60.0	$4.0\ 10^7$	o (10^{-7})
Dust-devils	3.0	10.0	$5.0\ 10^6$	o (10^{-6})
Whirl pools	15.0	5.0	$7.5\ 10^7$	o (10^{-7})
Aerodynamic	1.0	10.0	$6.7\ 10^5$	o (10^{-5})

Table 2.1.1 shows us various types of vortex and the corresponding magnitude δ.

Under the previous assumptions, the equation of motion in cylindrical coordinates is shown in the Fig. 2.1.1. Neglecting the terms of δ or smaller and simplifying the above equations are reduced into:

Continuity:

$$\frac{1}{r}\frac{d}{dr}\left(r V_r\right) + f\left(r\right) = 0 \tag{2.1.1}$$

Radial, *r*- momentum:

$$\frac{V_\theta^{\,2}}{r} = \frac{d\Delta\Pi}{dr} \tag{2.1.2}$$

Axial, *z* - momentum:

$$\frac{d\Delta\Pi}{dz} = 0 \tag{2.1.3}$$

The above equation of axial momentum shows us the dimensionless static pressure does not vary in the axial direction. Therefore, the pressure must be only a function of z.

Tangential θ-momentum:

$$\frac{V_r}{r}\frac{d}{dr}\left(r\,V_\theta\right) = \frac{1}{\mathrm{Re}}\frac{d}{dr}\left\{\frac{1}{r}\frac{d}{dr}\left(r\,V_\theta\right)\right\} \tag{2.1.4}$$

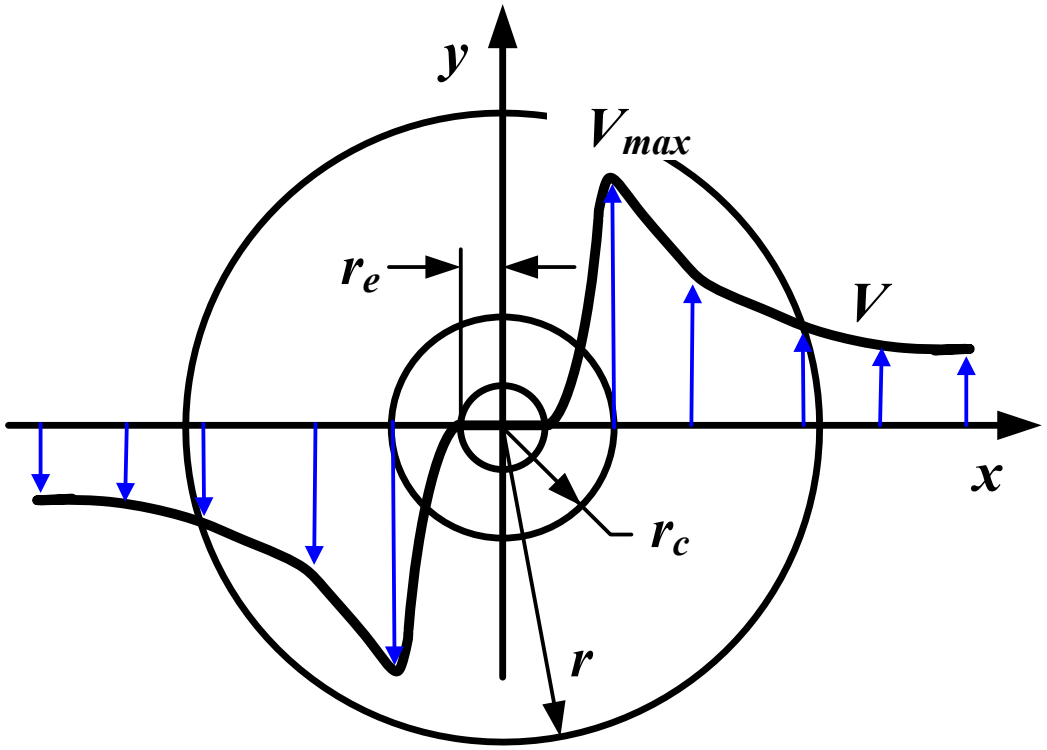

Figure 2.1.2 Typical tangential velocity profile for a multi-cell vortex.

Where,

$r=r^*/r_c^*$.

$z=z^*/r_c^*$.

$V_\theta=V_\theta^*/V_c^*$.

$V_r=V_r^*/V_c^*$.

$V_z=V_z^*/V_c^*$.

$\Delta p = (p^* - p^*_o) / \rho^* V^{*2}_c$.

$\Delta p_\infty = (p^*_\infty - p^*_o) / \rho^* V^{*2}_c$.

$\Delta\Pi = \Delta p/\Delta p_\infty$,

$Re = \Gamma_\infty{}^*/2\pi\nu^*$. (p^* is the pressure, p^*_∞ is the pressure far from the vortex center)

Subscript "c" label properties at the vortex core while the asterisk indicates that the specific quantities have dimensions**.**

2.2 Generalized Sullivan Two-Celled Vortices

Sullivan proposed a double cellular structure where within the inner cell there is a central downdraft in the axial, and a divergence of the flow in the radial directions [8]. These properties are displayed by negative and positive values of the axial and radial velocity components, respectively.

The original Sullivan is:

$$V_\theta^* = \frac{\Gamma_\infty}{2\pi r H(\infty)} H\left(\frac{ar^2}{2\nu}\right) \tag{2.2.1}$$

Where,

$$H^*\left(\beta r^2\right)=\int_0^r s\exp\left(-\int_0^s\left[-2\beta\, t+\frac{6}{t}\left(1-e^{-\beta t^2}\right)\right]dt\right)ds$$

$$H^*(\infty)=\lim_{r\to\infty}H\left(\beta r^2\right)$$

$$V_r^*=-ar+\frac{6\nu}{r}\left(1-e^{-\frac{ar^2}{2\nu}}\right) \tag{2.2.2}$$

$$V_z^*=2az\left(1-3e^{-\frac{ar^2}{2\nu}}\right) \tag{2.2.3}$$

The asterisk indicates that the specific quantities have dimensions**.**

Sullivan and others did not notice that, if the number 6 in the radial velocity by *m* (*m* is a constant), and then one can obtain a family of Sullivan vortices. This is possible since the intense vortex equations 2.2.1 to 2.2.3 represent an undetermined system.

With this modification the dimensionless radial and axial velocity equations become:

$$U=\mathrm{Re}V_r=\frac{V_r^*\,2\pi\,\mathrm{Re}}{\Gamma_\infty^*}=-2\beta\, r+\frac{m}{r}\left(1-e^{-\beta r^2}\right) \tag{2.2.4}$$

$$W=f\left(r\right)\mathrm{Re}=\frac{V_z}{z}=\frac{V^*{}_z\,2\pi\,\mathrm{Re}}{\Gamma_\infty{}^*\,z}=-2\beta\,\left(2-m\,e^{-\beta r^2}\right) \tag{2.2.5}$$

The tangential velocity is:

$$V_\theta = \frac{V_\theta^* 2\pi r_c^*}{\Gamma_\infty^*} = \frac{1}{r}\frac{H\left(\beta r^2\right)}{H(\infty)} \tag{2.2.6}$$

Where:

$$H\left(\beta r^2\right) = \int_0^r s \exp\left(-\int_0^s \left[-2\beta\, t + \frac{m}{t}\left(1 - e^{-\beta t^2}\right)\right] dt \right) ds$$

Here, s is dummy variable

and

$$H(\infty) = \lim_{r\to\infty} H\left(\beta r^2\right)$$

But, the maximum tangential velocity should occur at $r = 1$,

or $\left[\frac{dV_\theta}{dr}\right]_{r=1} = 0$

Application of the previous constraint in Eq. 2.2.6 yields:

$$\exp\left(-\int_0^1 \left[-2\beta\, t + \frac{m}{t}\left(1 - e^{-\beta t^2}\right)\right] dt \right) -$$

$$\int_0^1 s \exp\left(-\int_0^s \left[-2\beta\, t + \frac{m}{t}\left(1 - e^{-\beta t^2}\right)\right] dt \right) ds = 0 \tag{2.2.7}$$

Given m, the above equation is used to find β numerically. Then equation 2.2.6 along with 2.2.7 will yield the tangential velocity distribution for the Sullivan family of vortices with m = 6 being the classical Sullivan's formulation. All the numerical calculations and the code written to perform the calculations can be found in Appendix A.

The simplified tangential momentum is:

$$\frac{U}{r}\frac{d}{dr}(rV_\theta) = \frac{d}{dr}\left[\frac{1}{r}\frac{d}{dr}(rV_\theta)\right]$$

or

$$U\ Y = \frac{dY}{dr} \quad \text{Where, } Y = \frac{1}{r}\frac{d}{dr}(rV_\theta)$$

Then

$$\frac{dY}{Y} = \mathrm{U}\ dr$$

Separation of variables followed by integration yields

$$\ln Y = \int_0^r U\ dr + c_0$$

or

$$\frac{1}{r}\frac{d}{dr}(rV_\theta)= e^{\int_0^r U\,dr} \rightarrow \frac{d}{dr}(rV_\theta)= e^{\int_0^r U\,dr}\ r \ \rightarrow\ d(rV_\theta)= e^{\int_0^r U\,dr}\ r\,dr$$

A second integration gives,

$$[V_\theta\ r]_r - [V_\theta\ r]_0 = \int_0^r e^{\int_0^r U\,dr}\ r\,dr$$

Since $[V_\theta\ r]_0$=0, then

$$V_\theta\ r = \int_0^r e^{\int_0^r U\,dr}\ r\,dr$$

or

$$V_\theta\ = \frac{1}{r}\int_0^r e^{\int_0^r U\,dr}\ r\,dr$$

Inserting the expression

$$U = -2\beta\, r + \frac{m}{r}\left(1 - e^{-\beta r^2}\right)$$

into the derived tangential velocity gives,

$$V_\theta = \frac{1}{r}\int_0^r e^{\int_0^r U\, dr}\, r\, dr$$

or

$$V_\theta = \frac{1}{r}\int_0^r x\, exp\left(\int_0^x \left[-2\beta\, s + \frac{m}{s}\left(1 - e^{-\beta s^2}\right)\right] ds\right) dx$$

Here both *x* and *s* are dummy variables.

As the above equation does not satisfy the condition:

$$\lim_{r\to\infty} V_\theta \; r \to 1$$

Therefore, in order to satisfy the last, the tangential velocity component becomes:

$$V_\theta = \frac{1}{r}\frac{\int_0^r x\, exp\left(\int_0^x \left[-2\beta\, s + \frac{m}{s}\left(1 - e^{-\beta s^2}\right)\right] ds\right) dx}{\int_0^\infty x\, exp\left(\int_0^x \left[-2\beta\, s + \frac{m}{s}\left(1 - e^{-\beta s^2}\right)\right] ds\right) dx}$$

The term

$$\int_0^\infty x\, exp\left(\int_0^x \left[-2\beta\, s + \frac{m}{s}\left(1 - e^{-\beta s^2}\right)\right] ds\right) dx$$

Which represents a constant and as such the tangential velocity component satisfies the original differential equation in the azimuth direction:

$$\frac{U}{r}\frac{d}{dr}(rV_\theta) = \frac{d}{dr}\left\{\frac{1}{r}\frac{d}{dr}(rV_\theta)\right\}$$

Since Sullivan's formulation is based on Burgers' solution, Burgers'vortex will be obtained at the limit as *m* in the extended Sullivan's approaches zero ($m \to 0$):

Radial velocity

$$U = \mathrm{Re}V_r = -2\beta r$$

Axial velocity

$$W = f(r)\mathrm{Re} = 4\beta$$

Tangential velocity

$$V_\theta = \frac{1}{r}\left[1-\exp(-\beta r^2)\right]$$

Where,

$$\beta = 1.25643$$

Table 2.2.1 the values of β for different m (constant).

m	β
0	1.2564
2	2.5756
4	4.4248
6	6.2381
10	9.4433
20	16.4688

Given m, the value of β is calculated solving Eq. 2.2.7 numerically. Table 2.2.1 provides the β values for different m.

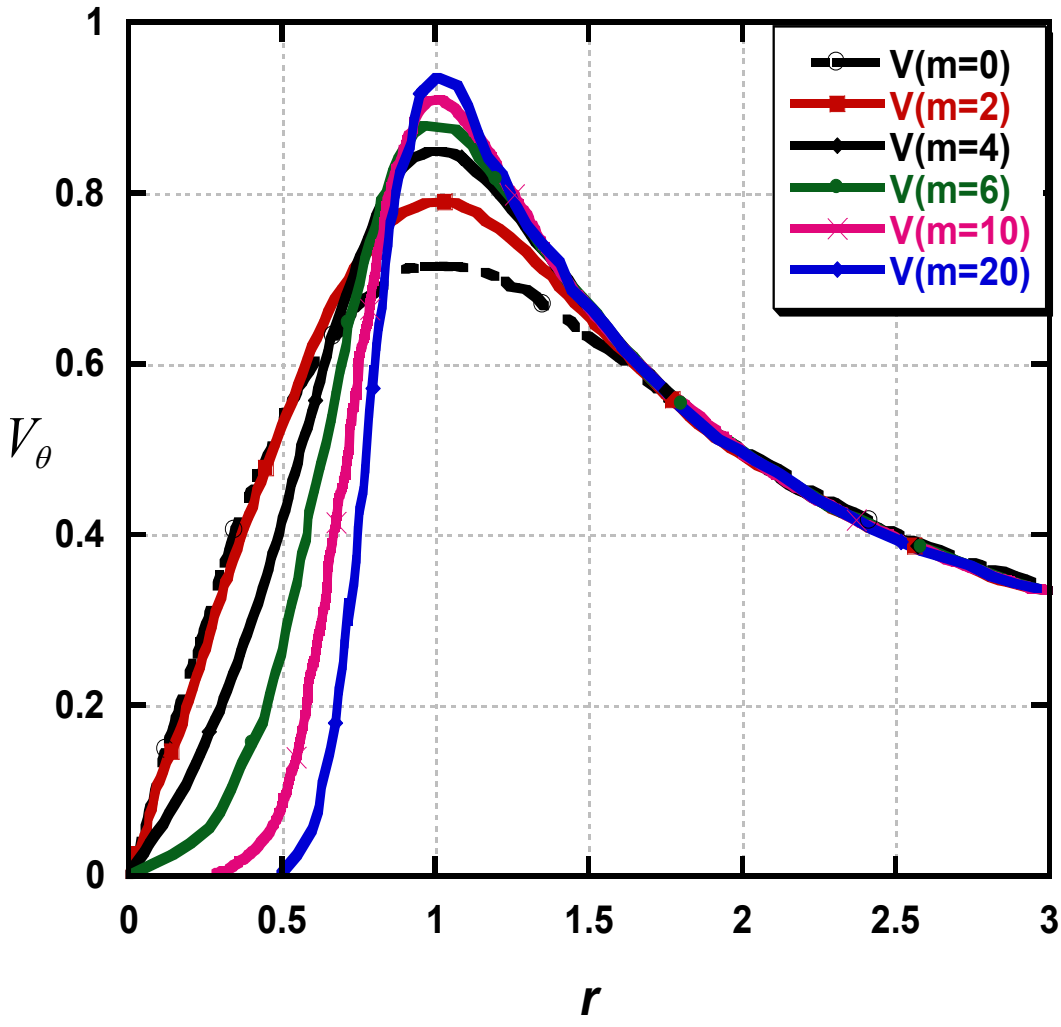

Figure 2.2.1 Tangential velocity profiles for different values of m.

Tangential velocity distributions for various values of *m* are given in Fig. 2.2.1. It is evident that the grater the value of *m* is, the more the concavity of the velocity distribution in $0 \leq r \leq 1$. In fact for large *m* values one can observe

the "eye" of the vortex evolving. The size of the "eye" enlarges as the value of *m* increases. Unfortunately, as it will be shown next, this formulation being a descendant of Burgers produces radial velocity profiles that are unbounded in *r*.

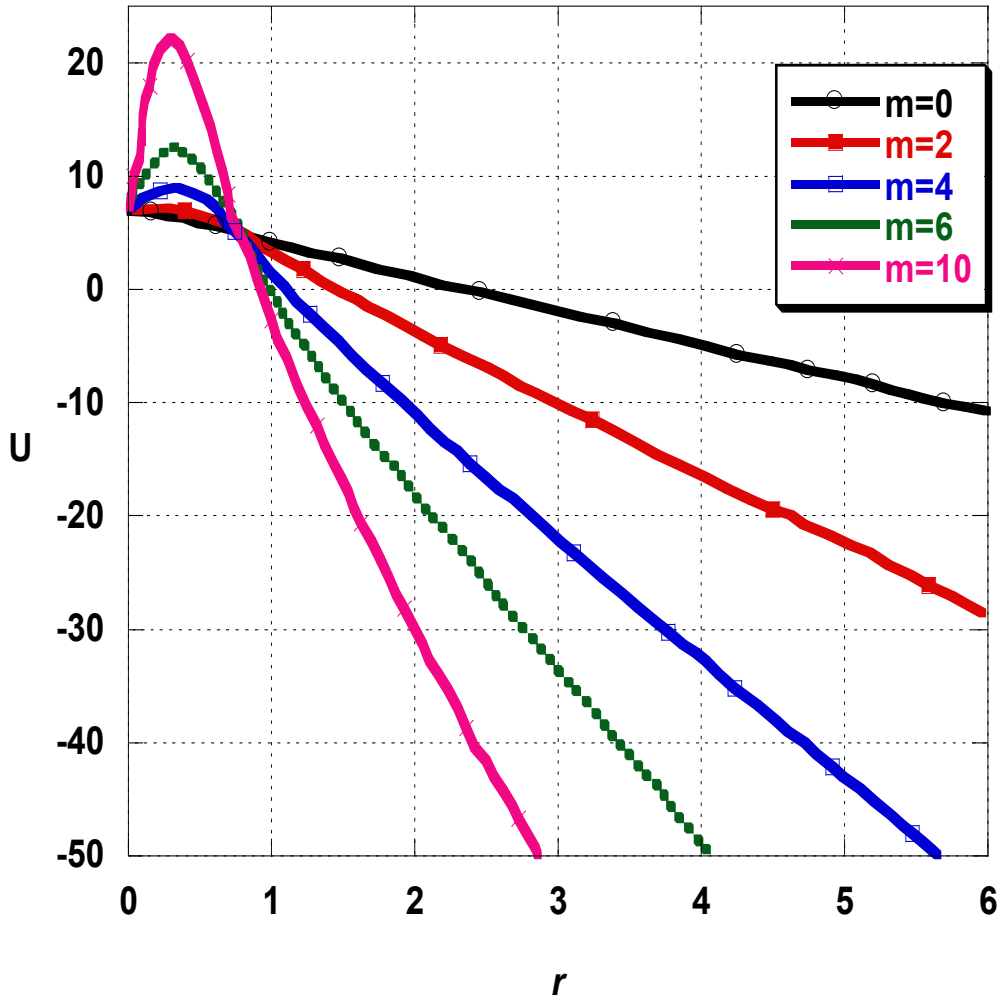

Figure 2.2.2 Radial velocity profiles for different values of m.

In Fig. 2.2.2 the radial velocity profiles for various values of *m* are presented. When m = 0 classical Burgers' velocity evolves, while when *m* = 6 the original Sullivan's radial velocity appears. The rate of growth of the radial velocity far from the center increases with the value of *m*. As illustrated in Fig. 2.2.3 the same is also the case with the axial velocity profiles. In this case however the far field constant value of the axial velocity increases with *m*.

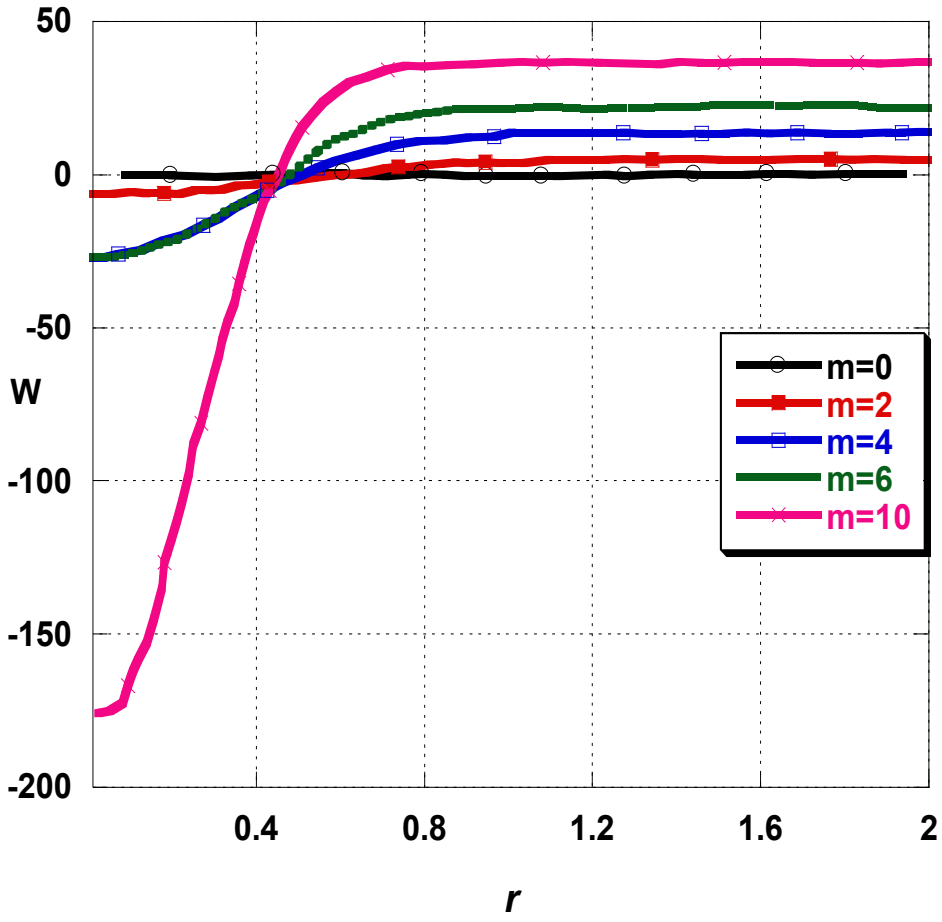

Figure 2.2.3 Axial velocity profiles for different values of m.

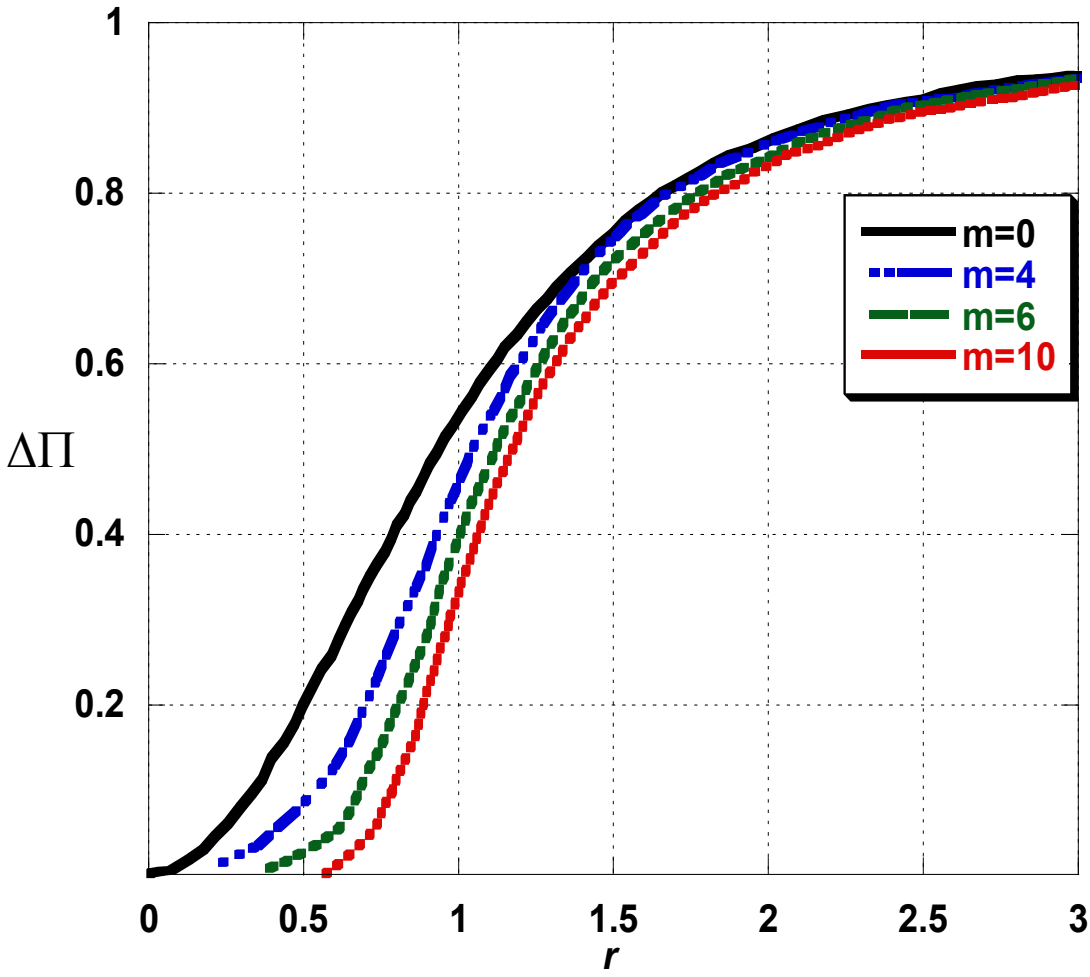

Figure 2.2.4 Static pressure profiles for different values of m.

The overall pressure profile for different values of m is shown in Fig. 2.2.4. Once more the classical vortices of Burgers and Sullivan appear for m = 0 and 6 respectively. Also, inside the vortex "eye", where the velocity is almost zero, the pressure profile is flat.

It is important to note that more mathematically involved developments of the generalized Sullivan vortex can be found in Gilliam et al. (2003) [10], Mickel (2000) [11], and Baker, J. T. (2000) [12].

2.3 The New Multi-Celled Vortices

The 1959 Sullivan's vortex accounted for one case of a double-cell meridional flow. The work of Vatistas (1998) produced a family of two-cell flow field [4]. Here the original contributions of multi-celled vortices are explained. In an attempt to incorporate this behaviour, the following generalized Vatistas [4] axial velocity profile is suggested:

$$\frac{V_z}{z} = 2\alpha \prod_{i=1}^{N} \frac{(-1)^{i+1}\kappa_i}{\left(1+\beta_i r^2\right)^2} \tag{2.3.1}$$

Where, N is the parameter that indicates the number of cells, α is arbitrary constant and β is scaling constant.

From continuity equation (2.1.1) the radial velocity component is,

$$V_r = -\alpha \sum_{i=1}^{N} \frac{\kappa_i (-1)^{i+1} r}{1+\beta_i r^2} \tag{2. 3.2}$$

Inserting the above expression into the θ-momentum equation (2.1.4) and after a double integration realizing also that $V_\theta\, r \to 1$ as $r \to \infty$, the general form of the tangential velocity component is obtained,

$$V_\theta = \frac{1}{r} \int_0^r \left\{ \prod_{i=1}^{N} \left[1 + \beta_i\, r^2 \right]^{\eta_i} \right\}^{\lambda} r\, dr \,/\, Y_\infty \tag{2.3.3}$$

Where,

$$Y_\infty = Y\left(r \to \infty\right) = \lim_{r\to\infty} \int_0^r \left\{ \prod_{i=1}^{N} \left[1 + \beta_i\, r^2 \right]^{\eta_i} \right\}^{\lambda} r\, dr$$

$$\eta_i = \frac{\kappa_i \left(-1\right)^i}{\beta_i} \quad \text{and}$$

$$\lambda = \frac{\alpha\, \mathrm{Re}}{2}$$

The requirement that the maximum velocity must occur at r = 1, yields the following,

$$\left\{ \prod_{i=1}^{N} \left[1 + \beta_i\, r^2 \right]^{\eta_i} \right\}^{\lambda} - \int_0^1 \left\{ \prod_{i=1}^{N} \left[1 + \beta_i\, r^2 \right]^{\eta_i} \right\}^{\lambda} r\, dr = 0 \tag{2.3.4}$$

The value of the root (λ) is found numerically solving the equation (2.3.4) in Maple 14 software. Here, only the smallest positive roots for various κ_2 values are calculated.

The axial-momentum equation (equation 2.1.3) suggests that the pressure does not vary along the axial direction. The pressure is then obtained from the radial momentum equation (equation 2.1.2).

$$\Delta\Pi = \frac{\int_0^r \frac{V_\theta^{\,2}}{r}\, dr}{\lim_{L\to\infty} \int_0^L \frac{V_\theta^{\,2}}{r}\, dr} \tag{2.3.5}$$

Where,

$$\Delta\Pi = \frac{p^* - p_0^*}{p_\infty^* - p_0^*}$$

According to the preceding equation it is worthwhile to remark that the diffusion of vorticity is balanced by that carried by the converging radial flow.

The vorticity component in the axial direction is given by:

$$\Omega_z = \frac{1}{r}\frac{d}{dr}\left(r\, V_\theta\right) = \left\{ \prod_{i=1}^{N} \left[1 + \beta_i\, r^2\right]^{\eta_i} \right\}^{\lambda} / Y_\infty \tag{2.3.6}$$

Where, $\Omega_{\mathbf{z}} = \Omega_z^*\, r_c^*/V_c^*$.

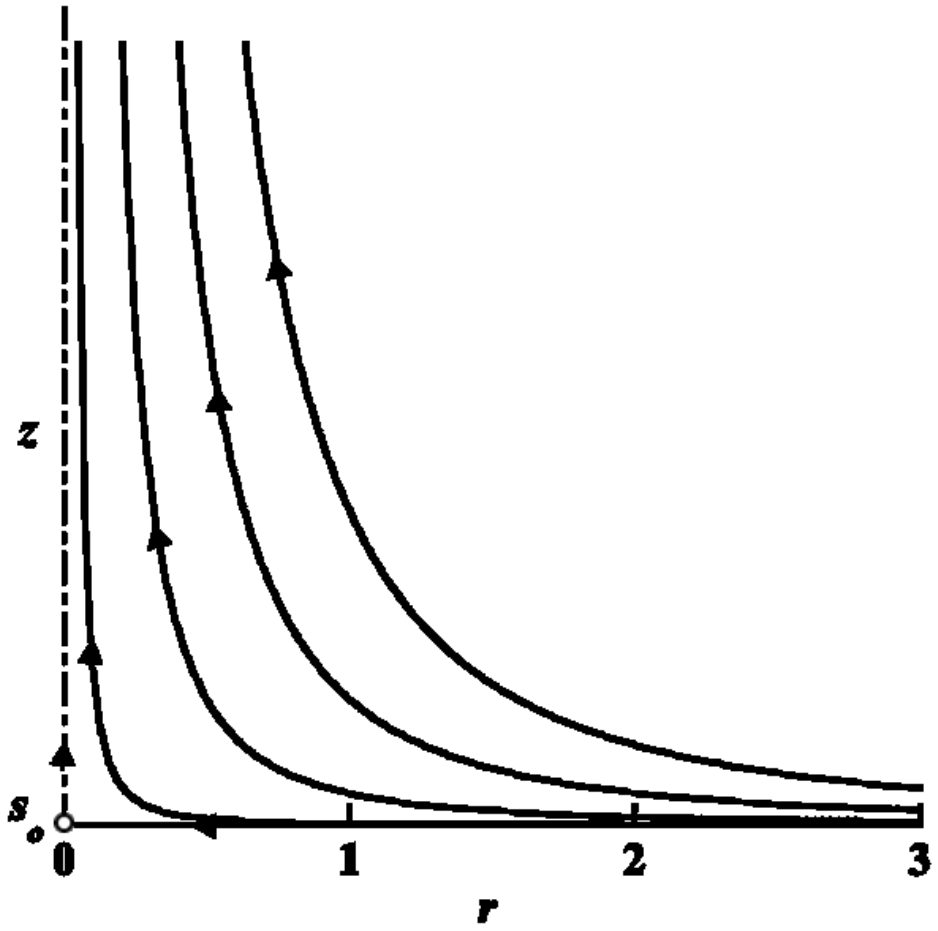

Figure 2.3.1 Schematic of the meridional flow pattern in the *r* - *z* plane for one-celled vortices.

A typical schematic of the meridional flow for one-cell vortex is shown in Fig. 2.3.1. In addition, Rankine, Kaufmann-Scully, Burgers vortex models are assumed one-celled vortex with the general flow pattern in the *r* - *z* plane [5, 6 and 7].

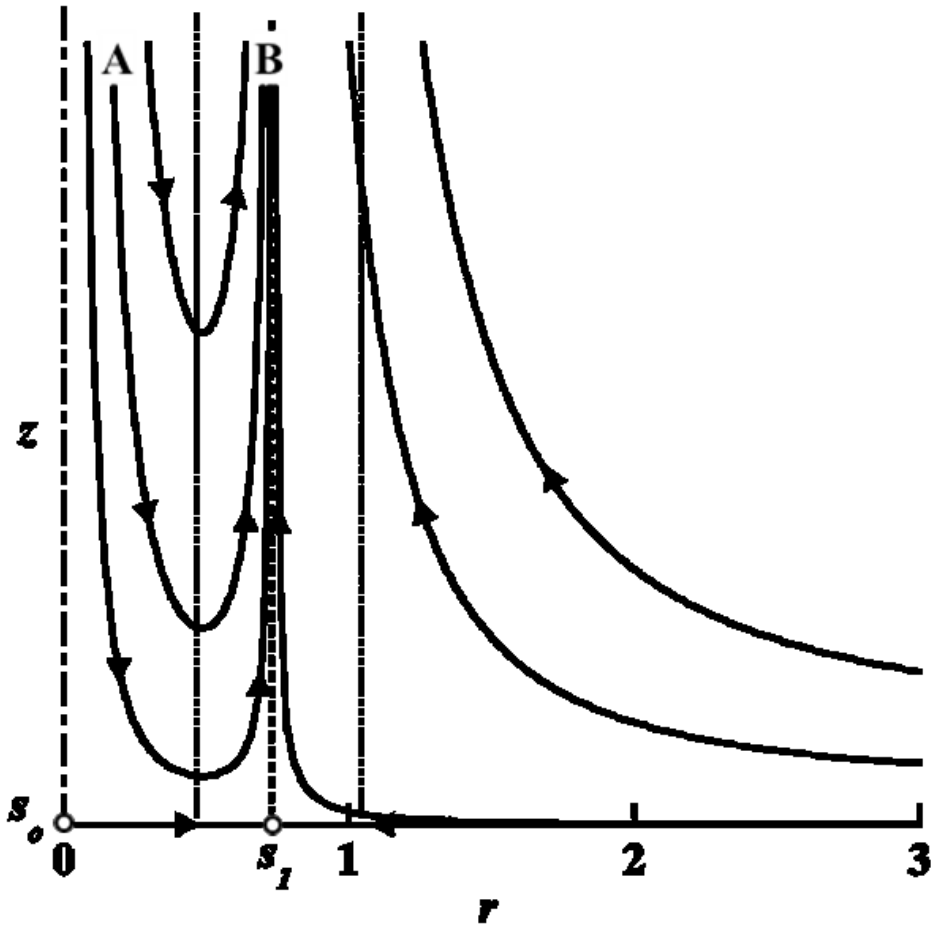

Figure 2.3.2 Schematic of the meridional flow pattern in the *r* - *z* plane for two-celled vortices.

Sullivan proposed a two-celled vortex characterized by a direction reversal of the radial and axial- velocity components near the axis of rotation. A schematic of the meridional flow pattern in the *r* - *z* plane for two-celled vortices is provided in Fig. 2.3.2.

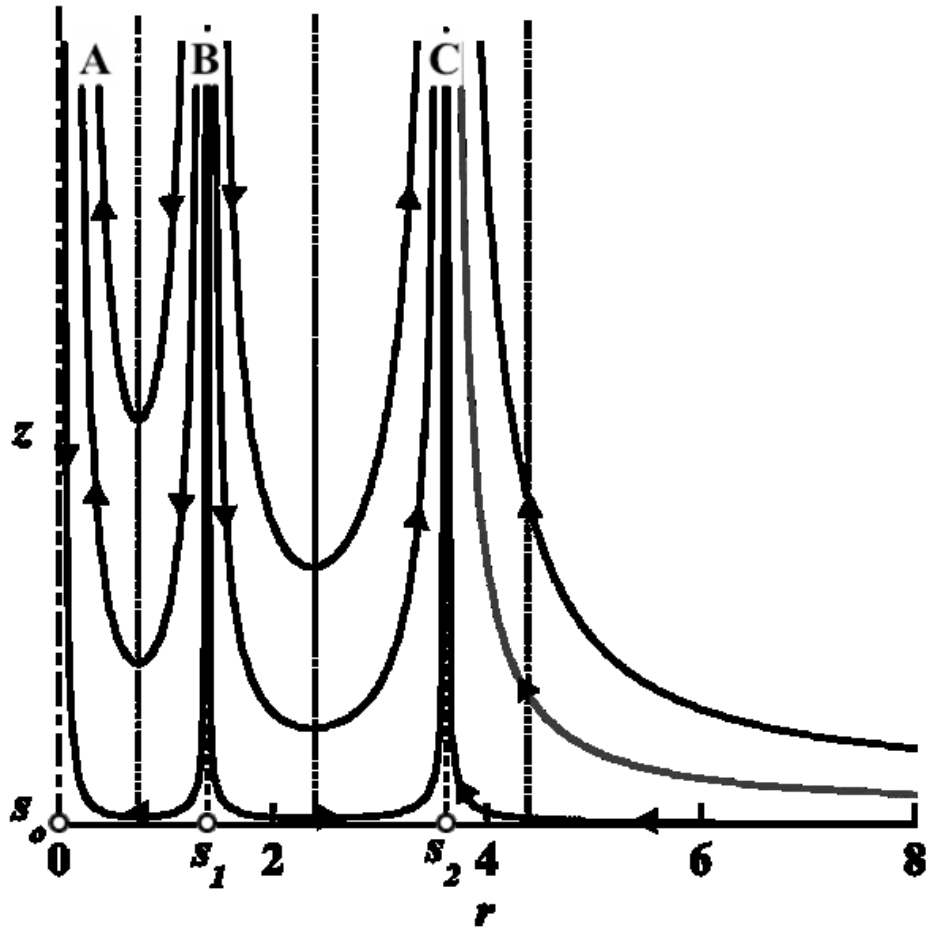

Figure 2.3.3 Schematic of the meridional flow pattern in the *r* - *z* plane for three-celled vortices.

Three and four cells are given in Figs. 2.3.3, and. 2.3.4 respectively.

The present study provides a new multi-celled vortices model, where one with a proper choice of the scaling parameters can generate single to *N*-celled intense vortices.

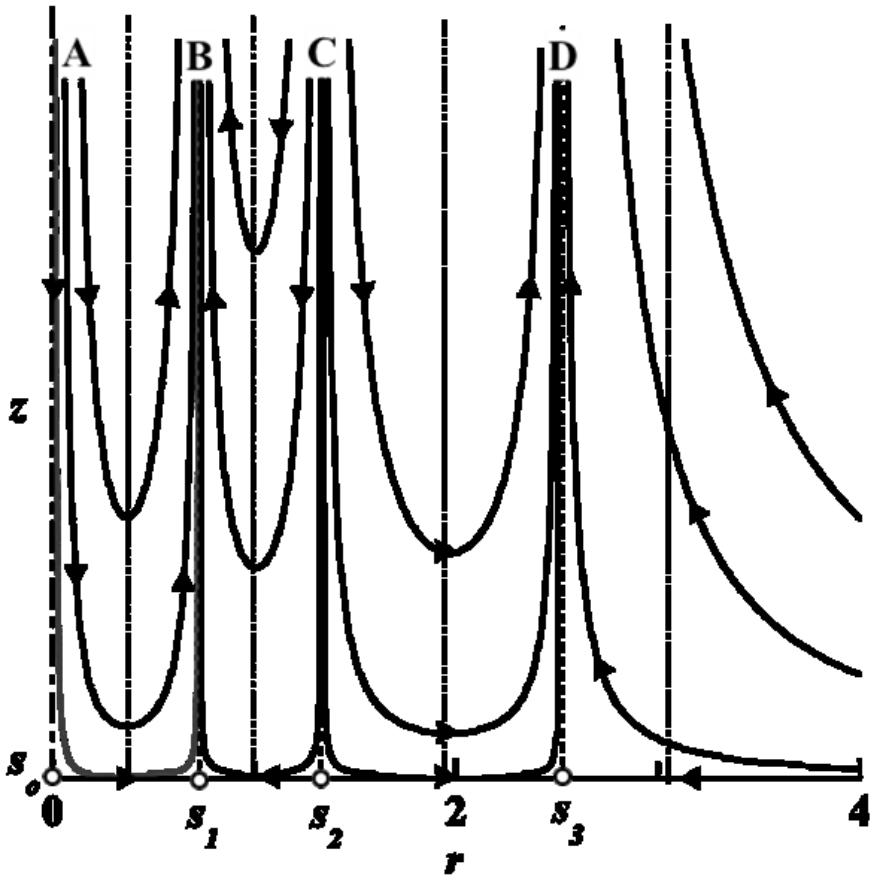

Figure 2.3.4 Schematic of the meridional flow pattern in the *r* - *z* plane for four-celled vortices.

Chapter 3 Numerical Solution

3.1 Methodology

The tangential, radial and axial velocity equations of multi-celled vortex are derived in the chapter 2. Static pressure and vorticity equations were also provided. The presentation of results for $N = 2$ begins by setting the scaling parameters as follows:

$\kappa_1 = 1$,

$\beta_1 = 0.375$,

$\beta_2 = 0.6$, and vary κ_2.

The values of κ_1, β_1, and β_2 were given before by Vatistas (1998) after a great deal of parametric examination [4].

The value of λ is then calculated via equation 2.3.4. The solution is obtained using MATLAB and Maple 14 code. The codes can be found in Appendices A and B.

Next, Y_∞ is evaluated and then it is insert into equation 2.3.3 to obtain the tangential velocity profile. The radial component of the velocity is obtained from equation 2.3.2 while equation 2.3.1 provides the axial velocity profile. Equations 2.3.5 and equation 2.3.6 furnish the static pressure and vorticity correspondingly. Table 3.1.1 contains the value of the calculated parameters, which are needed for the specific calculations.

Table 3.1.1 Important scaling parameters of tangential velocity

of present vortex model.

κ_2	λ	Y_∞	V_Θ *(at the peak, r =1)*
0.6	3.3069	0.4041	0.666
0.8	5.3847	0.4082	0.698
1.0	15.7418	0.4553	0.777

1.08	52.8349	0.9307	0.869
1.10	**111.1532**	**4.3713**	**0.913**
1.12	318.7127	8208.1328	0.951
1.13	474.8508	1166679.141	0.965

3.2 Mathematical Formulation of Multi Cellular Vortices

The profiles of the tangential velocity for different values of κ_2 = 0.6, 0.7, 0.8, 0.9, 1.0, 1.1, and 1.13 are plotted in Fig. 3.2.1. For $\kappa_2 \leq 1$ there is no change in the profiles within the inner part of the vortex core. When κ_2 increases further, the tangential velocity is formed a concavity near the center. Moreover, when the value of κ_2 is 1.1 a vortex-eye (area of almost zero velocity) begins to develop inside the core.

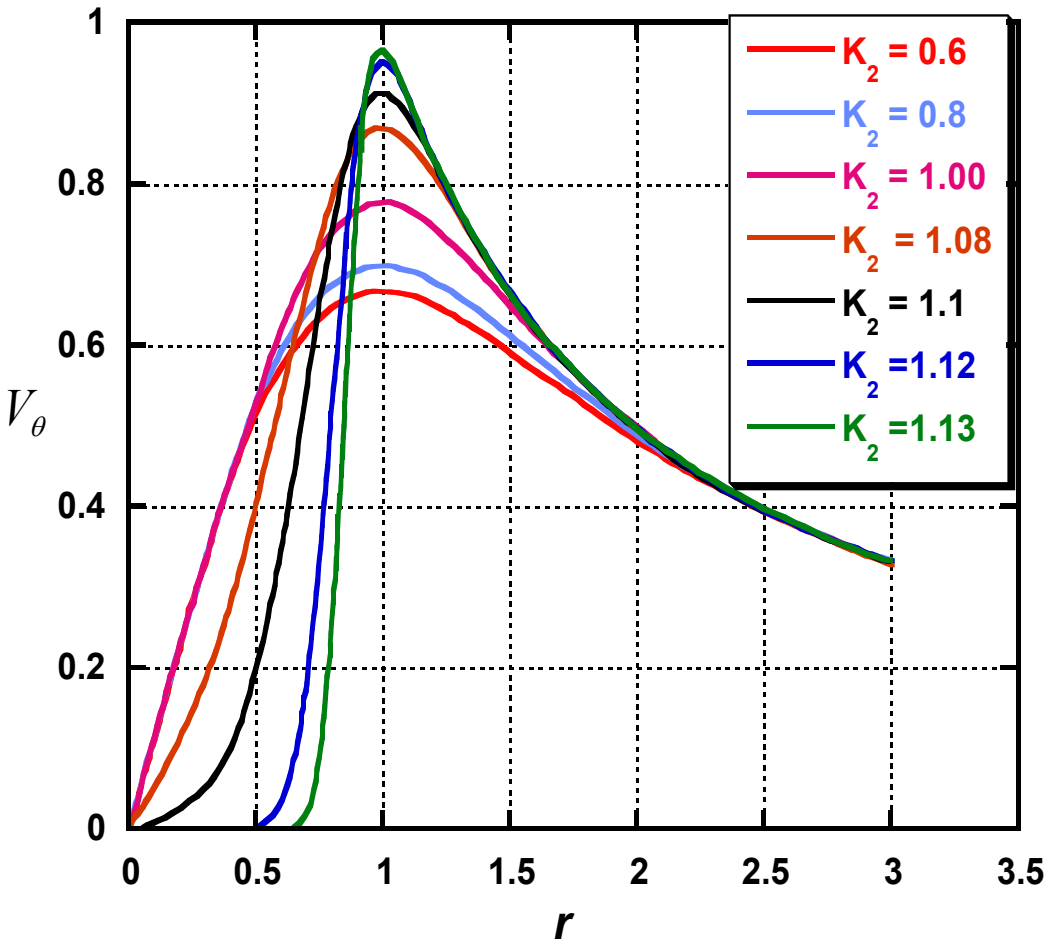

Figure 3.2.1 Profile of the tangential velocity of multi cellular vortices for different scaling parameters.

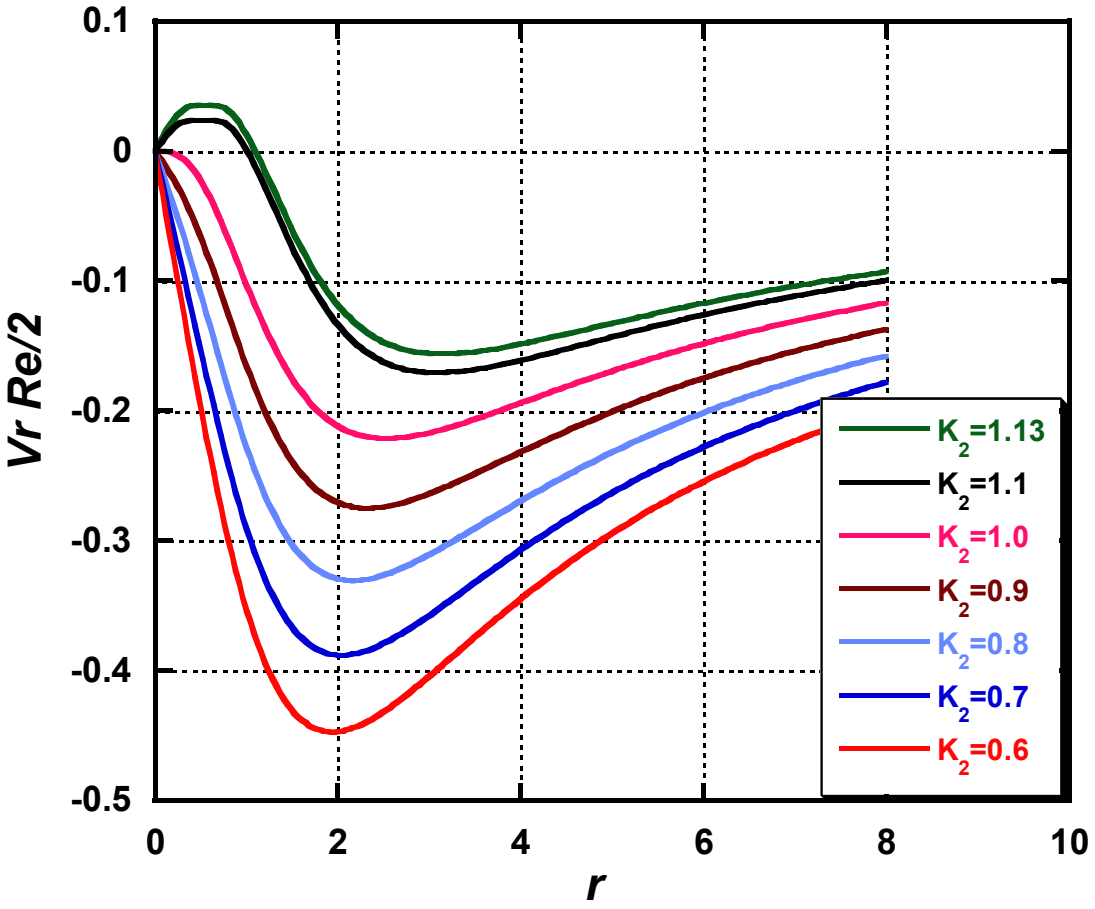

Figure 3.2.2 Profile of the radial velocity of multi cellular vortices for different scaling parameters.

Figure 3.2.2 shows that far away from the axis of rotation the radial velocity profile converges towards the center of the vortex. Furthermore, for $\kappa_2 \leq 1$ the value of the radial velocity is negative and vice versa for $\kappa_2 \geq 1.10$. On the other hand, inside the core the flow diverges for $\kappa_2 > 1$.

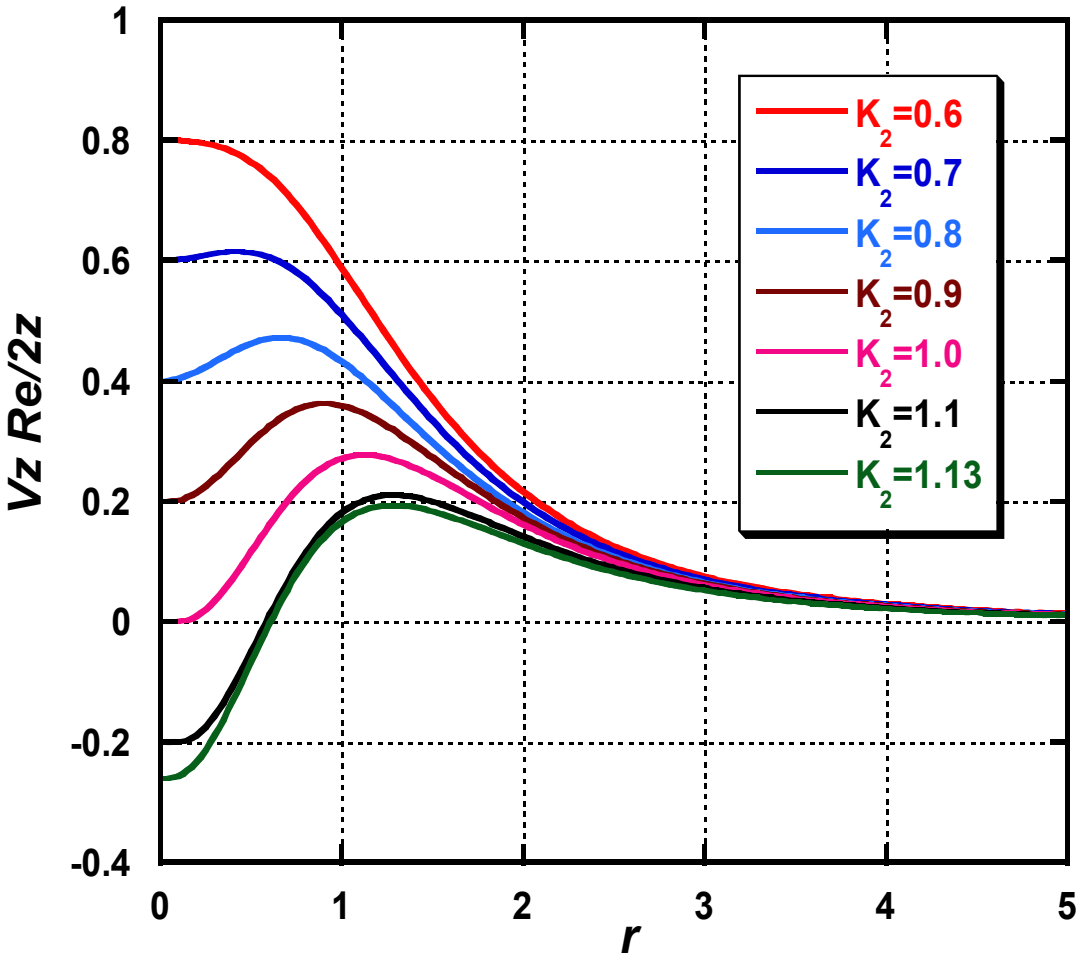

Figure 3.2.3 Profile of the axial velocity of multi cellular vortices for different scaling parameters.

The axial velocity profile is shown in Fig. 3.2.3. When, $\kappa_2 \geq 1.10$, this velocity produces a wake-like profile. On the contrary, κ_2 from 0.60 to 1, the axial velocity

develops a deficit at the axis of rotation and reaching the zero value when $\kappa_2 = 1$. It is interesting that the axial velocity component possesses a jet-like shape when $\kappa_2 = 0.6$.

Vorticity radial profiles are given in Fig. 3.2.4. The first characteristic to be noticed is that its maximum peaks occur always inside the core. From the same graph the vorticity is contained within the core, which is the trade-characteristic of concentrated vortices [13].

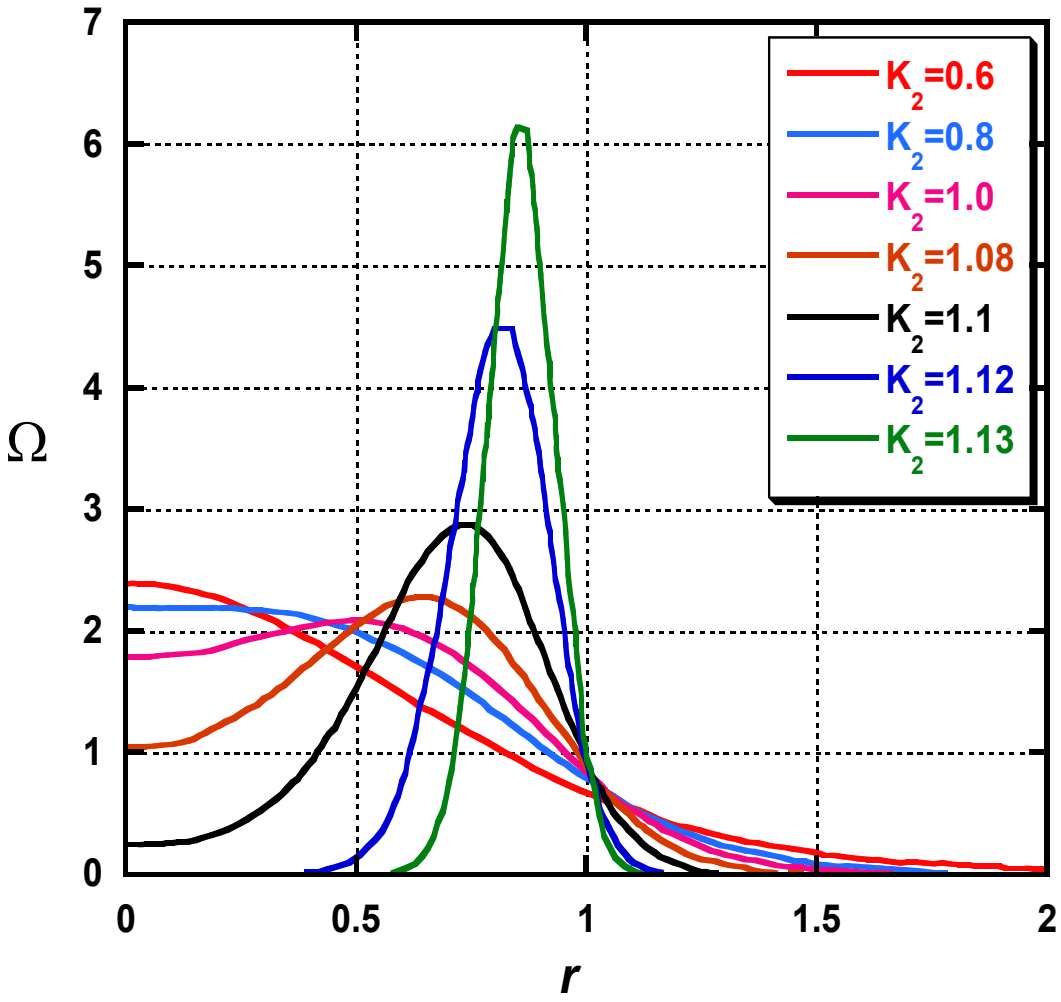

Figure 3.2.4 Profile of the vorticity of multi cellular vortices for different scaling parameters.

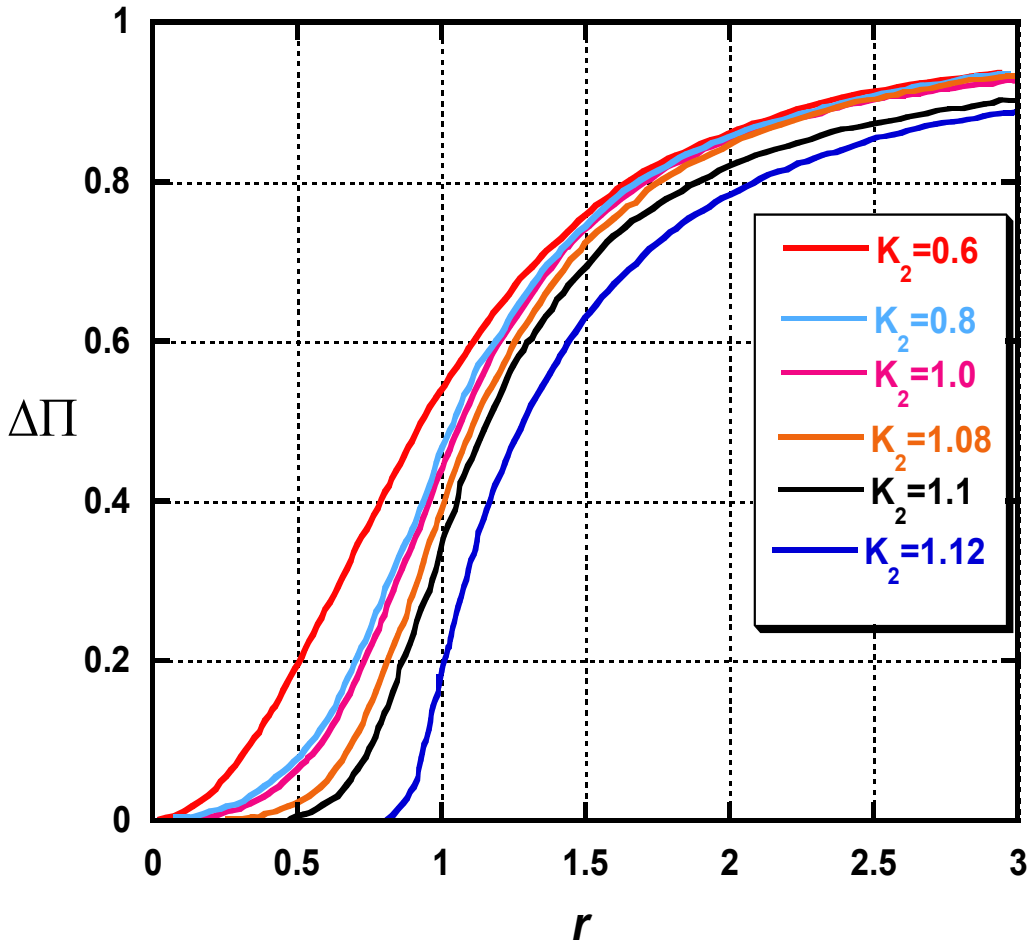

Figure 3.2.5 Profile of the static pressure of multi cellular vortices for different scaling parameters.

Static pressure distributions for different values of κ_2, are plotted in Fig. 3.2.5. It is clear from Fig. 3.2.5 that the static pressure exhibits a flat valley near the vortex center and the flat valley is the eye, because the tangential velocity is almost zero there.

Table 3.2.1 Percentage of vorticity (%) for the present vortex model.

κ_2 (When $\kappa_1 = 1, \beta_1 = 0.375, \beta_2 = 0.6$)	Percentage of vorticity (%)
0.6	66.71
0.8	69.85
1.0	77.76
1.08	87.22
1.10	91.42
1.12	95.65
1.13	97.51

The percentage of vorticity inside the core for the present multi cellular vortex model, as a function of κ_2 is shown in Table 3.2.1. Where, $\kappa_1 = 1$, $\beta_1 = 0.375$ and $\beta_2 = 0.6$. The percentage of vorticity is directly proportional to the value of κ_2.

The κ_2 value controls also the size of the vortex eye. As it is clearly illustrated in Fig. 3.2.6 the region where the velocity and hence vorticity is almost zero, expands outwards with κ_2.

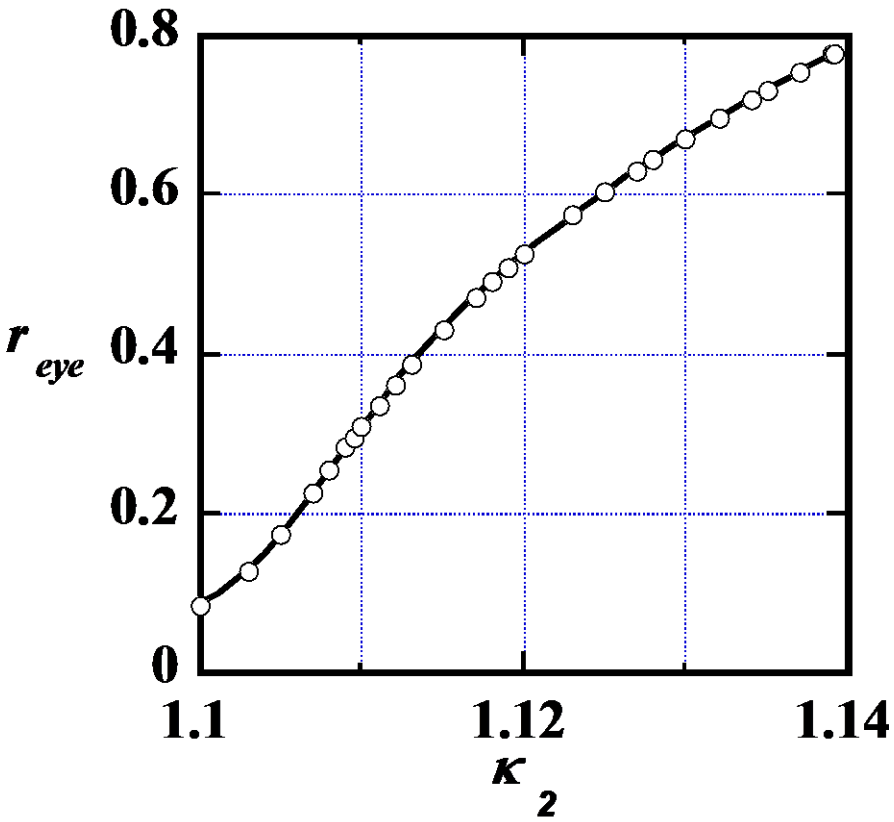

Figure 3.2.6 Vortex eye radius as a function of scaling parameter κ_2.

Chapter 4 Discussion of Results

In this section, using the present methodology, a sample of correlations of multi-celled (N = 2) atmospheric and aerodynamic vortices is presented. All the needed scaling parameters for these curve-fits are given in Tabular form. Here the new multi cellular vortex model is compared with experimental data of Dallas Tornado as well as Kansas Tornado [14, 15]. These two tornados are atmospheric vortices. The speed of the wind in the tornado has been a topic of continuous interest since many indirect ways have been used to estimate at least the maximum speed near the ground of tornadoes.

4.1 Correlations of Geophysical Vortices

4.1.1 Atmospheric Vortices

There are various kinds of atmospheric vortices such as, dust devils, tornadoes, and mesocyclones. Among those, only the tornado will be considered. This whirl is approximated by continuous functions that are zero at the vortex center, increase to a maximum at core radius, and then decrease asymptotically to zero infinitely far from the center.

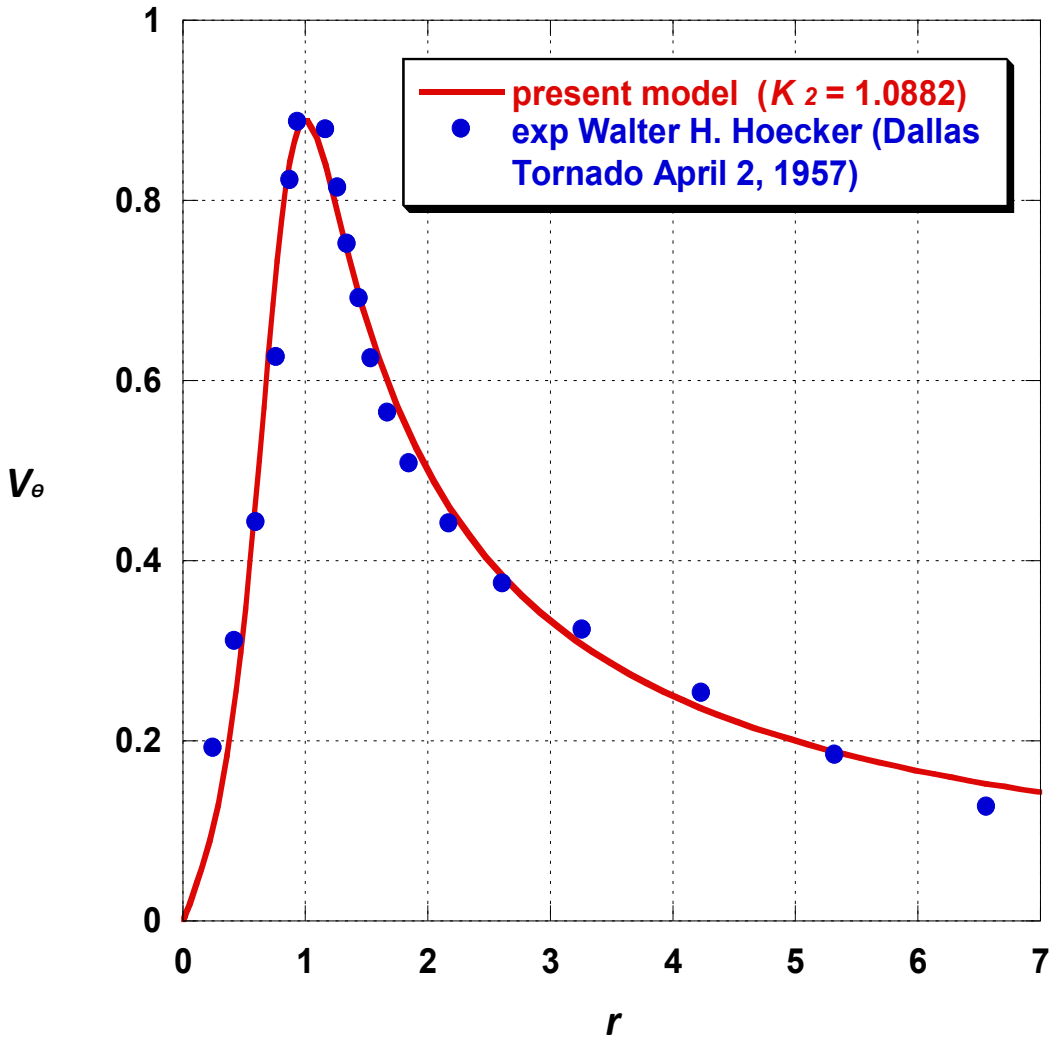

Figure 4.1.1 Comparisons of the tangential velocity with present multi-celled vortices model, (κ_2 = 1.0882) and experimental data of Walter H. Hoecker (Dallas Tornado April 2, 1957) [14].

The tangential component of wind around the Dallas tornado is discussed in the section. It is assumed; the tornado appeared to be in approximately the same stage of development, for most of the observations [14].

The data points are located where by chance tracer particles were located and that the highest speed measured was not necessarily the highest speed existing in the tornado. The multi-cell vortex model is compared with the Dallas tornado as a nondimensional form. We can observe from the Fig. 4.1.1 that by selecting suitable values for the scaling parameter, κ_2 = 1.0882 the present vortex model correlates reasonably the experimental data of the Dallas Tornado [14]. Other important scaling parameters are as follows:

λ = 70.1064

Y_∞ = 1.410

V_Θ = 0.913 (the value of the tangential velocity is at the pick, when r =1).

Kansas tornado of 15 May 1999 was collected by a mobile, 3-mm-wavelength, 95-GHz (W-band) Doppler radar high-resolution radar reflectivity and Doppler velocity data [16]. Data collection contained thirty-five scans of radar reflectivity and velocity

data during the entire life cycle of the tornado [15]. We are comparing the Kansas tornado with the present vortex model. All the Maple and Math lab cod are attached at the Appendix A and Appendix B.

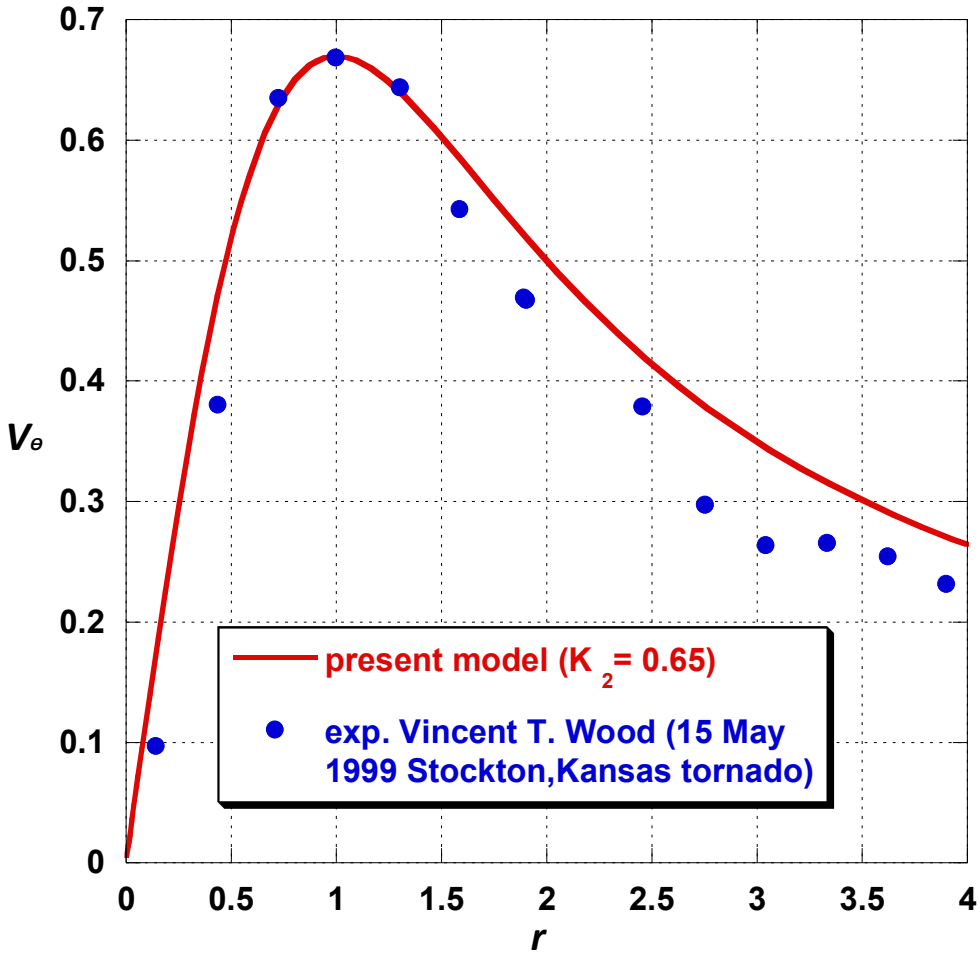

Figure 4.1.2 Correlations of multi-celled vortex model, (κ_2 = 0.65) and experimental data of Vincent T. Wood (Kansas Tornado May 15, 1999) [15].

For the best fit of Kansas Tornado with our multi cellular vortex model, all the scaling parameters were first calculated. The parameters are as follows:

$\kappa_2 = 0.65$

$\lambda = 3.7399$

$Y_\infty = 0.4047$

$V_\Theta = 0.690$ (the value of the tangential velocity is at the pick, when r =1).

Figure 4.1.2 compares the tangential velocity of our present model with the Kansas Tornado, with the scaling parameter of $\kappa_2 = 0.65$ was found to be more appropriate [15].

Table 4.1.1 shows us all the important scaling parameter of tangential velocity of atmospheric vortices, which are plotted in the Fig. 4.1.1 and Fig.4.1.2.

Table 4.1.1 Important scaling parameter of tangential velocity of Atmospheric Vortices [20].

Atmospheric vortices	κ_2	λ	Y_∞	V_θ ***(at the pick, r =1)***
Dallas Tornado April 2, 1957	1.0882	70.1064	1.4103	0.913
Kansas Tornado May 15, 1999	0.65	3.7399	0.4047	0.690

A large tornado occurred that caused F4-level damage was intercepted by the Doppler on Wheels (DOW) mobile radar near Mulhall, Oklahoma, on 3 May 1999 [17]. Three-dimensional structure of a tornado was deduced using the ground-based velocity track display (GBVTD) technique [18]. Pressure was deduced from the tangential and radial wind fields [19]. Now, the pressure profiles of Mulhall tornado with our present multi cellular vortex model is compared as well as calculated all the important parameters.

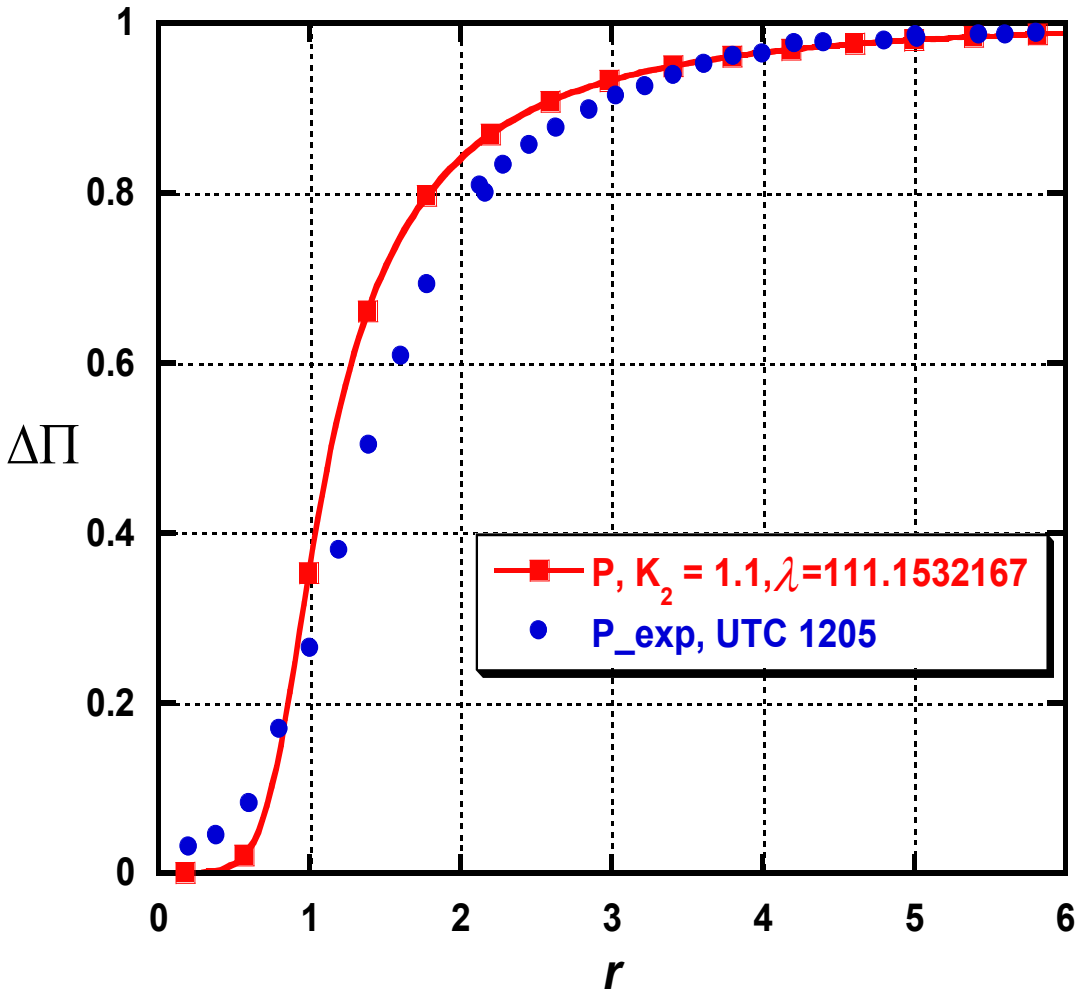

Figure 4.1.3 Comparisons of the static pressure with present multi-cell vortices model, (κ_2= 1.1) and experimental data of the Mulhall Tornado on 3 May 1999 [17].

The comparison of the Mulhall Tornado with our present model is provided in Fig. 4.1.3. All the important scaling parameters are calculated, here κ_2 was set at 1.1.

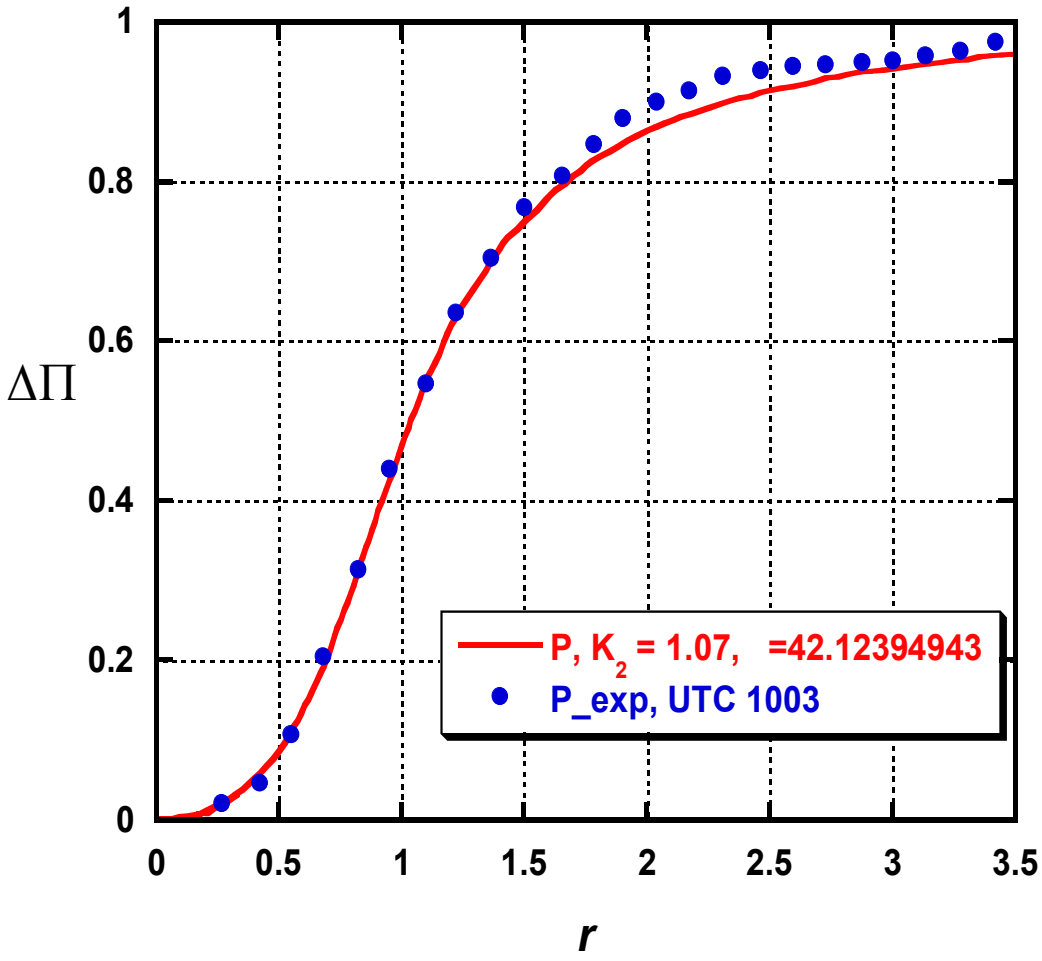

Figure 4.1.4 Comparisons of the static pressure with present multi-cell vortices model, (κ_2= 1.07) and experimental data of the Mulhall Tornado on 3 May 1999 [17].

The comparison of static pressure with the present model is provided in Fig. 4.1.4. The theoretical static pressure yielded a better match with the experimental data when κ_2 was taken as 1.07.

Table 4.1.2 Important scaling parameter of static pressure of Atmospheric Vortices (Mulhall Tornado on 3 May 1999) [20].

Atmospheric vortices	κ_2	λ	Y_∞
Mulhall Tornado May 3, 1999	1.1	111.1532	4.3713
Mulhall Tornado May 3, 1999	1.07	42.1239	0.7352

Important scaling parameters for static pressure of Mulhall Tornado are presented in the Table 4.1.2.

4.1.2 Vortices Generated by Surface Wind Action

When wind is blowing on the surface of a liquid like the ocean it creates waves. Underneath these waves a multitude of vortices are generated near the air-water interface.

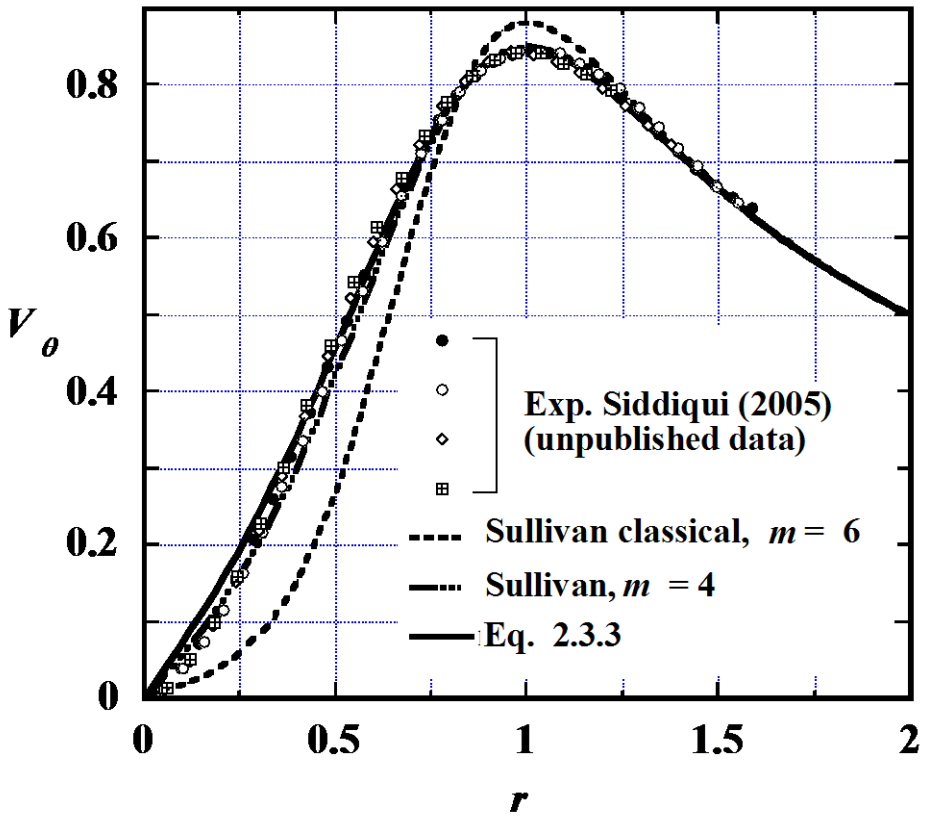

Figure 4.1.5 Two-cell vortices produced in a wind-wave flume.

The scaling parameters used in Eq. 2.3.3 are: $\beta_1 = 0.375, \beta_2 = 0.620$, $\kappa_1 = 1.000$, and $\kappa_2 = 1.072$.

Data collected in a wind-wave flume using a digital particle image velocimetry by Siddiqui (2005) [21]. Upon dimensionalization, a sample of 805 circular vortices, collapsed into a single curve. The experimental data given in Fig. 4.1.5 show good correlations with Eq. 2.3.3 and the generalized $m = 4$ Sullivan's theory.

4.2 Aerodynamic Vortices

Sample of correlations of multi-celled aerodynamic vortices with our present vortex model is compared. Aerodynamics vortices are important in a number of applications. It is a significant factor in any type of vehicle design, including automobiles. It is important in the prediction of forces and moments in sailing. It is used in the design of mechanical components such as hard drive heads. Structural engineers also use aerodynamics, and particularly in aeroelasticity, to calculate wind loads in the design of large buildings and bridges [22].

Next the present multi cellular vortex model is compared with two experimental aerodynamic vortices. All the needed scaling parameters for these curve-fits are given in tabular forms.

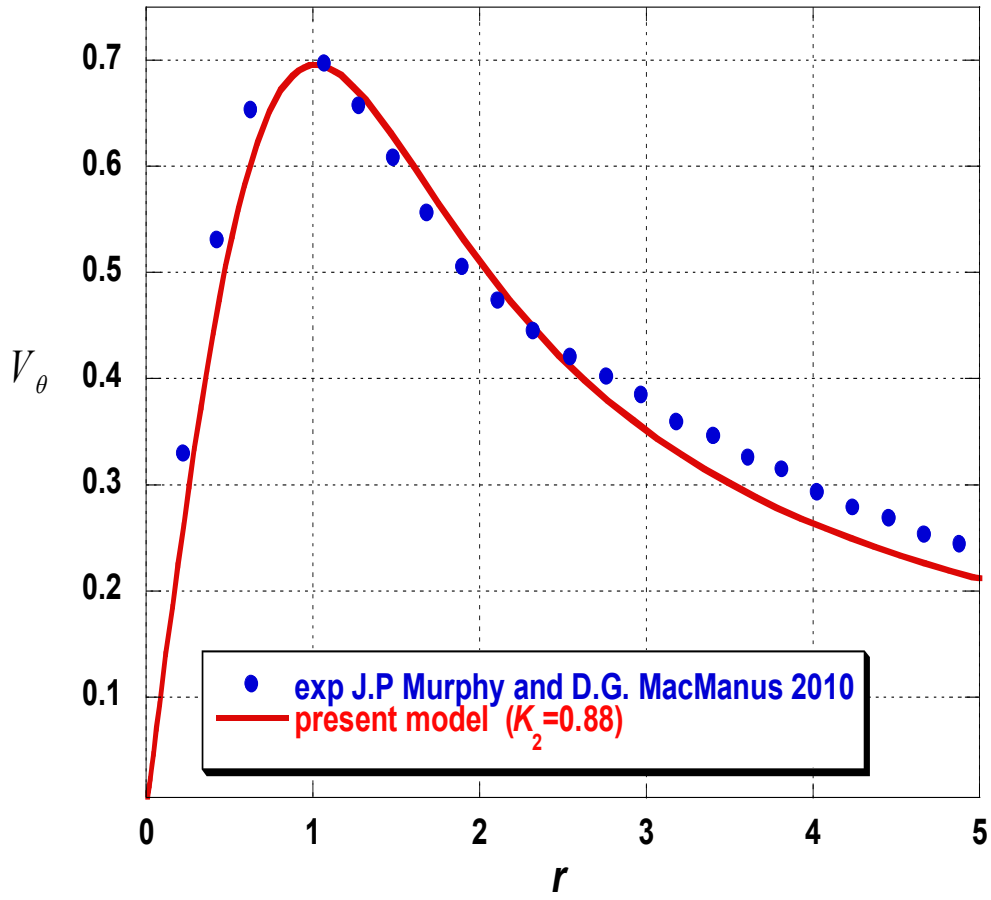

Figure 4.2.1 Comparisons of the tangential velocity with present multi-celled vortices model, (κ_2 = 0.88) and experimental data of J.P Murphy and D.G MacManus 2010 [23].

The tornado-like vortex, developed in front of the gas turbine intake, while the engine is operating at high power near the ground, can ingest foreign objects that cause pressure asymmetry, produce vibration and noise, and could also cause severe damage [23].

Figure 4.2.1 illustrates the correlations of the present vortex model for the aerodynamic vortices given in references. For this Figure the scaling parameter is $\kappa_2 = 0.88$.

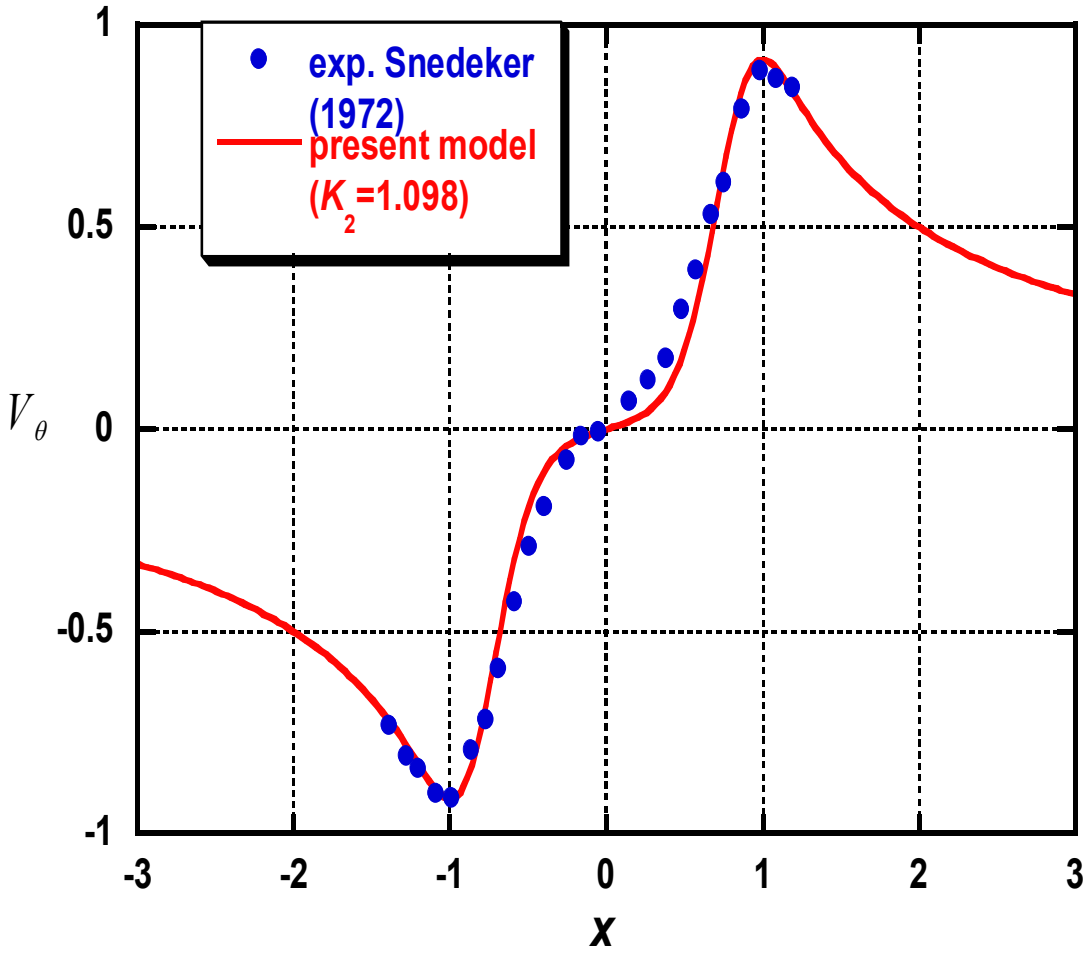

(a)

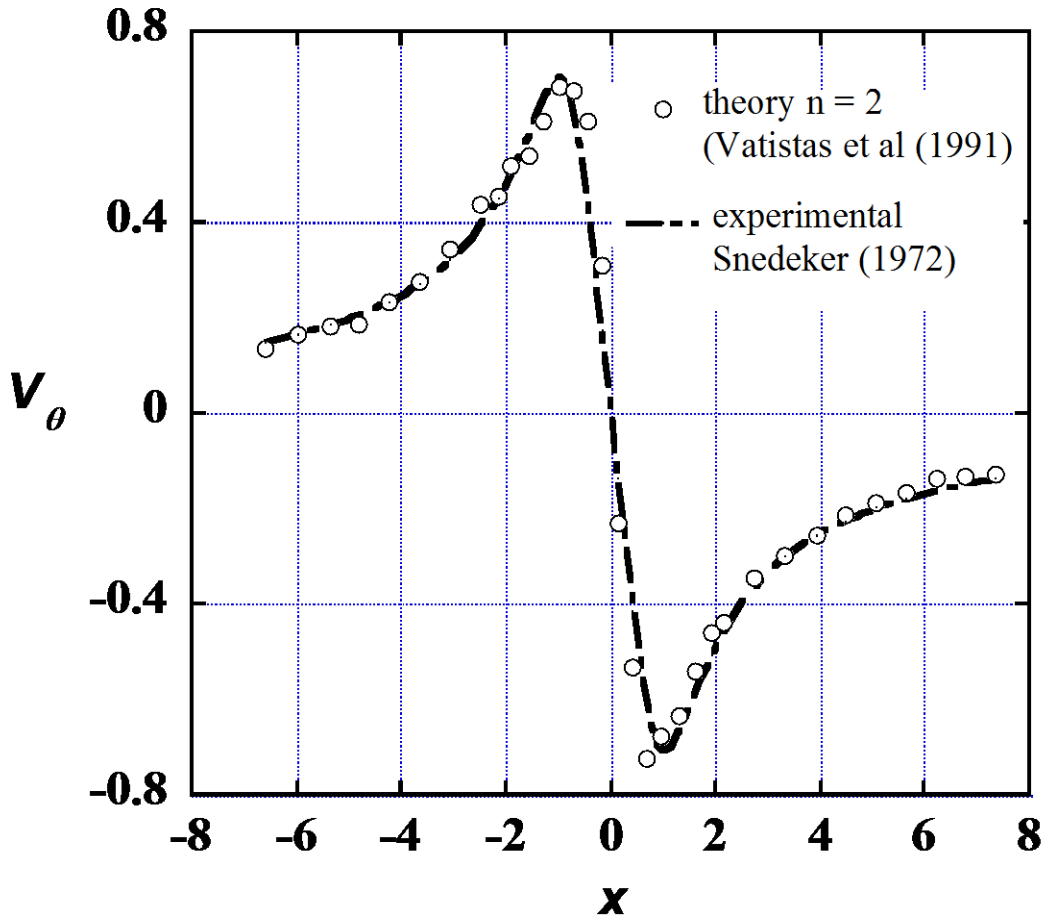

(b)

Figure 4.2.2 Comparisons of the tangential velocity for (a) two cells (κ_2 = 1.098) and (b) one cell with the experimental data of Snedeker (1972) [2]

One way to weaken the wake of an aircraft wing is to introduce an axial jet in the

proximity of the tip vortex inception [2]. Snedeker wind-tunnel experimental results show that the originally one cell tip-vortex transforms into two-cell type by introducing the axial jet. Figure 4.2.2 (a) illustrates the correlations of the present vortex model for the aerodynamic vortices given in reference [2]. For comparison the single-cell vortex (produced without axial jet) is shown in Figure 4.2.2 (b).

Table 4.2.1 Important scaling parameter of tangential velocity of Aerodynamic Vortices [20].

Aerodynamic vortices	κ_2	λ	Y_∞	V_Θ *(at the pick, r =1)*
Experimental data of J.P Murphy and D.G MacManus 2010	0.88	5.9471	0.4539	0.699
Snedeker (1972)	1.098	109.1375	3.4107	0.9128

Essential scaling parameters for tangential velocity of aerodynamic vortices are presented in the Table 4.2.1. [20]. The Table gives us details idea.

4.3 Vortex with 4 Cells

Until now most of the results presented pertained to two-cell vortices. This preference had as a base the fact that most of the evidence *vis-à-vis* multi-celled vortices were related to the latter kind. Here one representative example of a simulated four-cell whirl is given with $\beta_1 = 0.1$, $\beta_2 = 0.2$, $\beta_3 = 0.785$, $\beta_4 = 5$, $\kappa_1 = 1$, $\kappa_2 = 2$, $\kappa_3 = 2$ and $\kappa_4 = 2$.

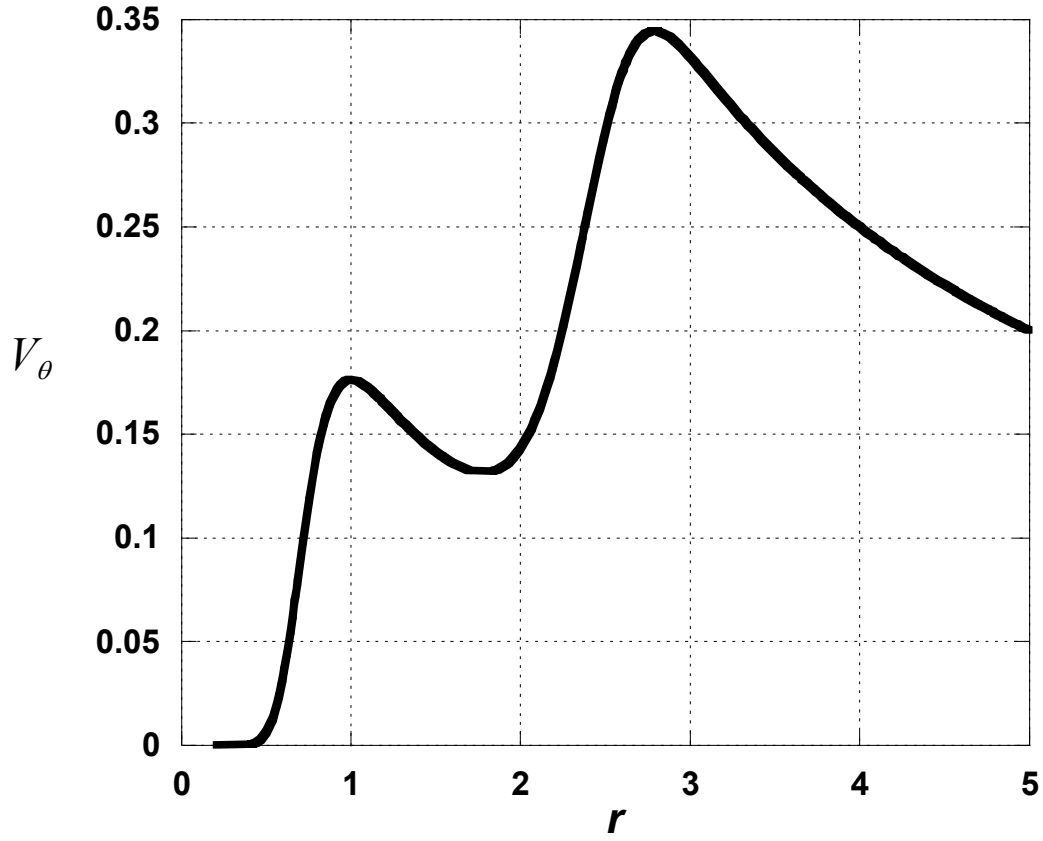

Figure 4.3.1 Tangential velocity for a case of four-cell vortex.

The tangential velocity profile shown in Fig. 4.3.1 indicates the presence of multiple maxima (two peaks).

The radial velocity provided in Fig. 4.3.2 show the converging flow from far field caries vorticity in the negative *r*-direction (V_r is negative), which replenishes that diffused (see θ-momentun equation, Eq. 2.1.4),

$$V_r \, \Omega = \frac{1}{\mathrm{Re}} \frac{d\Omega}{dr}$$

This is keeping the vortex steady. There are as many *r*-intercepts of the radial velocity curve as the number (*N*) of cells. At the base of the vortex the axial velocity is zero ($z = 0$). Therefore, there must be *N* stagnation points in the radial-axial flow $\left(V_r = V_z = 0\right)$. Note that the tangential velocity due to free-slip condition for $z = 0$ will not be zero. All velocities will be approximately equal to zero inside the "eye" because $V_\theta \sim 0$ in $0 \le r \le r_{eye}$, while V_r and $V_z \sim 1/\mathrm{Re}$ (the vortex Reynolds number for intense vortices ~ 4.0×10^7)

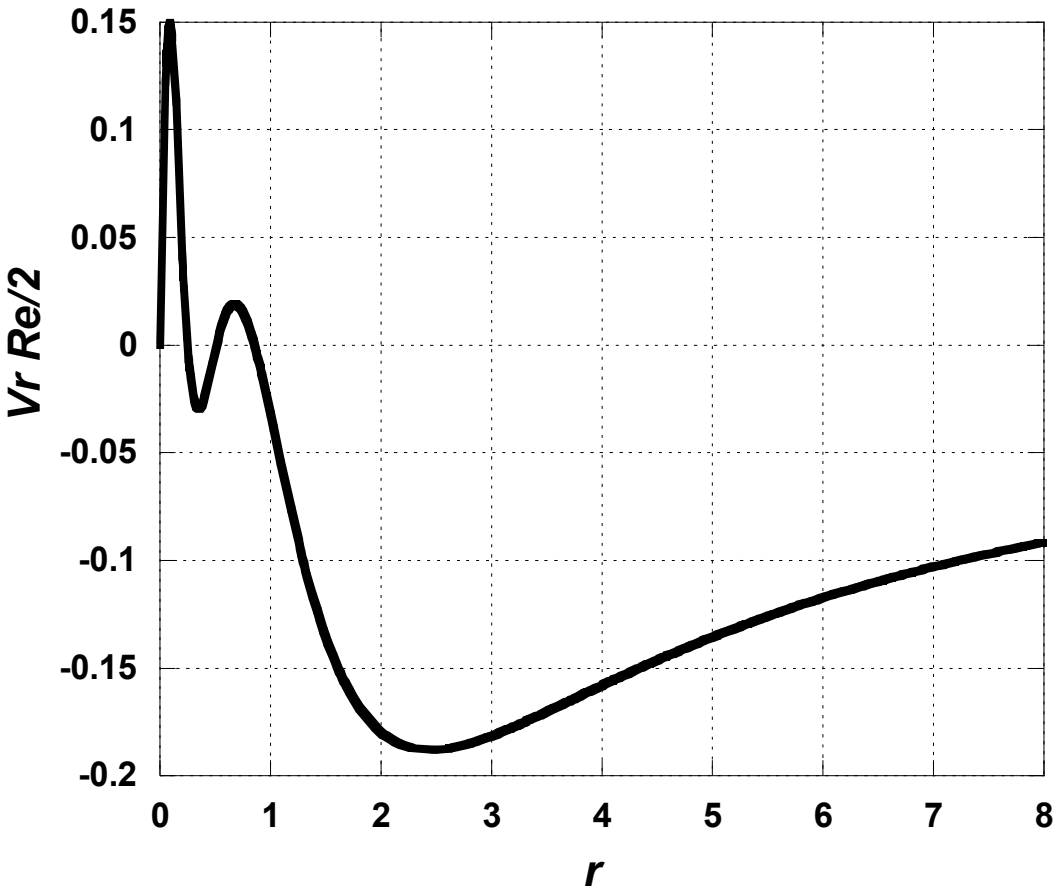

Figure 4.3.2 The radial velocity for a case of four-cell vortex.

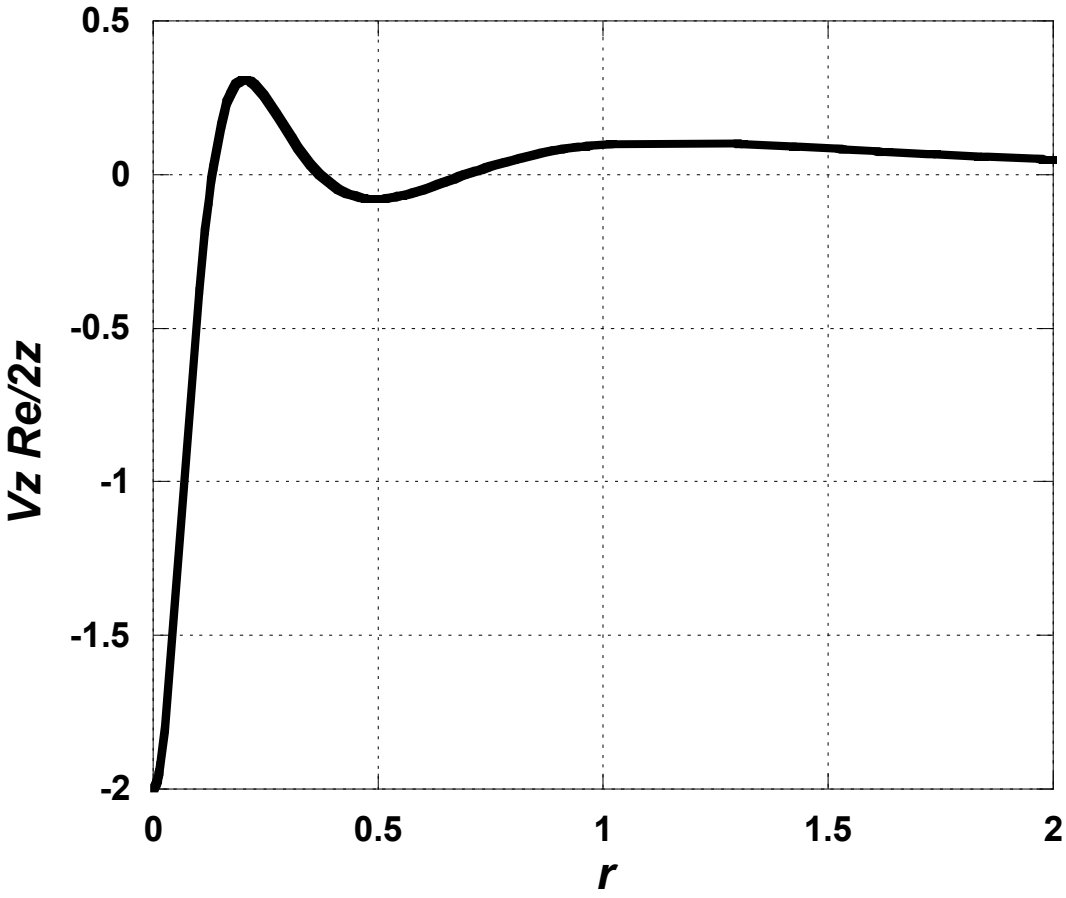

Figure 4.3.3 The axial velocity for a case of four-cell vortex.

The axial velocity distribution is given in Fig. 4.3.3. Responding to continuity the axial velocity peaks (both positive and negative) corresponds to *N*.

Here only one case of $N = 4$ was given. There is no doubt that a more extensive study is required. This is outlined in the section Future Work that is to follow.

Conclusions

In this investigation a new multi-cell vortex model, able to describe a variety of geophysical and aerodynamic multi-celled vortices was presented. The numerical results obtained using MATLAB and Maple 14 code confirmed by curve fitting actual observations of the tangential velocity and static pressure of geophysical and mechanically produced vortices. The methodology is kept simple, easy to understand, and general enough to be used in various future applications.

Selecting suitable values for the scaling parameters, the present theory correlate well the velocity, pressure, and vorticity distributions of multi cell vortices such as tornadoes, wind driven near the interface ocean whirls intake of gas turbines operating near the ground, and wing-tip-vortices.

In addition, the observed tangential velocity peaks detected in Hurricane Frances (2004) that were identified in the flight-level aircraft data were discussed in context of a simulated four-cell vortex.

Future Work

The present analysis can be further explored in various ways. Here are some ideas about next steps of our analysis:

- In this study the multi cellular vortex model is considered as steady, axisymmetric, incompressible vortex model. For the next step we can develop the analysis for unsteady as well as compressible fluid flow.

- Our present vortex formulation is capable to simulate multi-cell vortex but for this study most of the numerical calculations are done for mainly the two cell category. Future work should examine the fluid mechanical properties of three cell vortices or more.

References

[1] Carrier, G. F., Dergarabedian, P. and Fendell, F. E. "Analytic Studies on Satellite Detection of Severe, Two-Cell Tornadoes," NASA Contractor Report 3127, 1979.

[2] Snedeker, R.S, "Effect of Air Injection on the Torque Produced by a Trailing Vortex," *Journal of Aircraft,* **5,** No. 9, pp. 682-684, 1972.

[3] Phillips, W. R., "Turbulence Prediction and Measurement in a Turbulent Trailing Vortex," M.Eng. Thesis, McGill University, Department of Mechanical Engineering, 1974.

[4] Vatistas, G. H., "New model for intense self-similar vortices," *AIAA, Journal of Propulsion and Power*, **14**, No. 4, pp. 462-469, 1998.

[5] Rankine, W. J. M., "Manual of applied mechanics," C. Griffen Co., London, England, 1858.

[6] Kaufmann, W., "Über die Ausbreitung kreiszylindrischer Wirbel in zähen (viskosen) Flüssigkeiten," Ingenieur-Archiv **31**, No. 1, pp. 1-9, 1962. Also Scully, M. P., "Computation of Helicopter Rotor Wake Geometry and Its Influence on Rotor Harmonic

Airloads," Massachusetts Institute of Technology Report No. ASRL TR 178-1, March 1975.

[7] Burgers, J.M., "A mathematical models illustrating the theory of turbulence," Adv. in *App. Mech.*, **1**, pp. 171-199, 1948.

[8] Sullivan, R. D., "A Two-cell vortex solution of the Navier-Stokes equations," *Journal of the Aerospace Sciences,* **26**, No. 11, pp. 767-768, 1959.

[9] Vatistas, G.H., V. Kozel, W. Minh, "A simpler model for concentrated vortices," *Exp. Fluids*, **11**, pp. 73-76, 1991.

[10] Gilliam, D. S., Shubov, V. I., Mickel, C. E., Baker, and Vugrin, E., "Generalized Donaldson-Sullivan Model of a Vortex Flow," Proceedings 11th International Conference on Wind Engineering, **2**, pp. 2713-2720, 2003.

[11] Mickel, C. E., "Donaldson-Sullivan Tornado Model," MS Thesis in Mathematics, Texas Tech University, 2000.

[12] Baker, J. T., "High Viscosity Solutions of the Navier-Stokes Equations Modeling a Tornado Vortex," MS Thesis in Mathematics, Texas Tech University, 2000.

[13] Bluestein, H. B. Weiss, C. C. &. Pazmany A. L., "Doppler radar observations of dust devils in texas," Wea. Rew. **132,** pp. 209-224, 2004.

[14] Walter H. Hoecker, JR., "Wind speed and air flow patterns in the Dallas tornado of April 2, 1957," Monthly weather reviews, 1960.

[15] Vincent T. Wood et al., "An analytical model of one and two–celled vortices: Preliminary testing," University of Oklahoma.

[16] Tanamachi, R. L., H. B. Bluestein, W.-C. Lee, M. Bell, and A. Pazmany, "Ground-based velocity track display (GBVTD) analysis of W-band Doppler radar data in a tornado near Stockton, Kansas on 15 May 1999," Wea. Rev. (In press), 2006.

[17] Wen–Chau Lee, Joshua Wurman, "Diagnosed Three-Dimensional Axisymmetric Structure of the Mulhall Tornado," National Center for Atmospheric Research, Boulder, Colorado, 3 May 1999.

[18] Davies-Jones, R. P., "Tornado dynamics, in Thunderstorm Morphology and Dynamics," 2nd ed., edited by E. Kessler, University of Oklahoma Press, Norman, pp. 197-236, 1986.

[19] Pauley, R. L., "Laboratory measurements of axial pressure in two-celled tornado-like vortices," J. *Atmos. Sci.*, **46**, pp. 3392–3399, 1989.

[20] Israt Jahan Eshita, Georgios H. Vatistas, "Analysis of New Multi Cellular Vortex Model Relevance to Atmospheric and Aerodynamic Vortices," ASME 2014 Fluids Engineering Summer Meeting (FEDSM2014) Chicago, Illinois, USA, Aug. 2 -7, 2014.

[21] Siddiqui, M.H.K., "Digital Particle Image Velocimetry for Circular Vortices near Water-Air Interface Generated by Wind-Driven Wave Action," Unpublished work, 2005.

[22] J.S. Green, "Forced response of a large civil fan assembly," Proceedings of

ASME Turbo Expo. Power for Land, Sea and Air, 2008.

[23] J.P. Murphy, D.G. MacManus, "Inlet ground vortex aerodynamics under headwind conditions," *Aerospace Science and Technology,* **15,** pp. 207–215, 16 December 2010.

Appendix A

1. Algebraic solution of tangential, axial and radial velocity of Sullivan vortex model in Maple 13:

For N=2, (2 cell vortices)
Here

$\kappa_1 = 1$, $\beta_1 = 0.375$, $\beta_2 = 0$ is used to get the perfect value of κ_2 and λ (have to calculate positive smallest root), which gives us perfect match with the experimental values.

Step 1: first of all the value of κ_2=1.0882, then put the value in to the equation, $\left\{\prod_{i=1}^{m}\left[1+\beta_i r^2\right]^{\eta_i}\right\}^{\lambda} - \int_0^1 \left\{\prod_{i=1}^{m}\left[1+\beta_i r^2\right]^{\eta_i}\right\}^{\lambda} r dr = 0$ and solves it to get the value of λ. Solving the equation and after calculation, we get λ =111.1532167.

Step 2: Now we know λ which we can use to solve the tangential velocity component. Here mechanical vortex model is shown below:

$$V_\theta = \frac{1}{r}\int_0^r \left\{\prod_{i=1}^{m}\left[1+\beta_i r^2\right]^{\eta_i}\right\}^{\lambda} r\, dr \Big/ \lim_{r\to\infty}\int_0^r \left\{\prod_{i=1}^{m}\left[1+\beta_i r^2\right]^{\eta_i}\right\}^{\lambda} r\, dr$$

We also solve the equation by using Maple 13 software. The equation is critical to solve so we have done it two steps, first we have to solve, $Y_\infty = Y(r\to\infty) = \lim_{r\to\infty}\int_0^r \left\{\prod_{i=1}^{m}\left[1+\beta_i r^2\right]^{\eta_i}\right\}^{\lambda} r dr$

Where, $\eta_i = \frac{\kappa_i (-1)^i}{\beta_i}$. Then we get the value of Y_∞. In the second part we have to solve $V_\theta = \frac{1}{r} \int_0^r \left\{ \prod_{i=1}^{m} \left[1 + \beta_i r^2 \right]^{\eta_i} \right\}^{\lambda} r\, dr / Y_\infty$.

- **Step 3:** After getting the perfect profile for the comparison of experimental data we have to extract all the data points from the Maple 13 software. So for that we write a code in Mat lab to get all the data points.

- **Step 4:** Now we have to run the Mat lab code to get all the data points of Vatistas' multi-cellular mechanical vortex model. On the other hand experimental data points are extracted from the Data Thief software, so we have to plot the 2 velocity profiles together. For that we write another code in Mat lab to plot the two graphs together.

- **Step 5:** Now we have to measure the differences between values predicted by the model and the experimental values. Here we use root-mean-square error (RMSE) method. Here the value of RMSE = 0.092, which is pretty good match. If the RMSE is very large then we have to guess the value of κ_2 and calculate the λ again and repeat the step 1 to step 5.

> $$\frac{\int_0^5 x\cdot e^{\left(\int_0^x \left(-2\cdot(6.2381\cdot t)+\frac{6\cdot\left(1-1\cdot e^{-1\cdot\left(6.2381\cdot(t^2)\right)}\right)}{t}\right)dt\right)}dx}{1}$$

$$\int_0^5 x\, e^{\int_0^x \left(-12.4762\, t+\frac{6\left(1-e^{-6.2381\, t^2}\right)}{t}\right)dt}\,dx$$

> *evalf*[5](**(1)**)

$$3.0381$$

> $$\frac{\int_0^r x\cdot e^{\left(\int_0^x \left(-2\cdot(6.2381\cdot t)+\frac{6\cdot\left(1-1\cdot e^{-1\cdot\left(6.2381\cdot(t^2)\right)}\right)}{t}\right)dt\right)}dx}{3.0381\cdot r}$$

$$\frac{0.3291530891\left(\int_0^r x\, e^{\int_0^x \left(-12.4762\, t+\frac{6\left(1-e^{-6.2381\, t^2}\right)}{t}\right)dt}\,dx\right)}{r}$$

> *smartplot*(**(1)**)

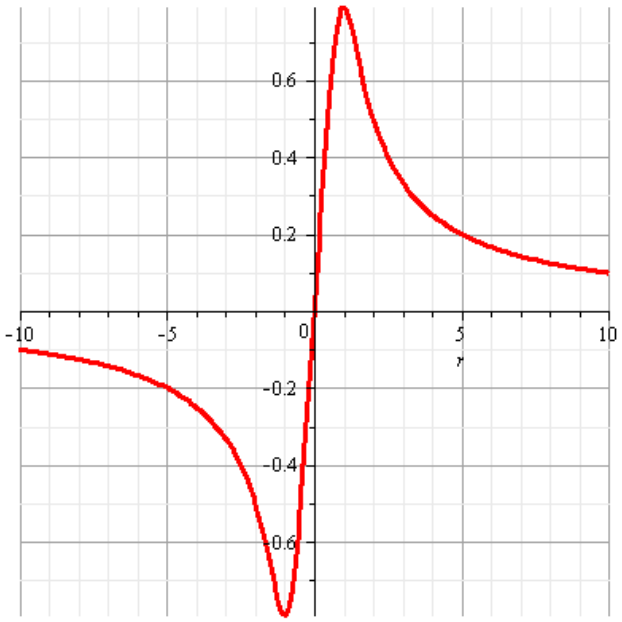

> $(-2\cdot 6.2381\cdot r)+\frac{6}{r}\cdot\left(1-e^{-6.2381\cdot r^2}\right)$

$$-12.4762\,r+\frac{6\left(1-e^{-6.2381\,r^2}\right)}{r}$$

> $4\cdot 6.2381-2\cdot 6\cdot 6.2381\cdot e^{-6.2381\cdot r^2}$

$$24.9524-74.8572\,e^{-6.2381\,r^2}$$

> $$e^{\left(\int_0^1\left(-2\,(b\cdot t)+\frac{4\cdot\left(1-e^{-b\cdot t^2}\right)}{t}\right)dt\right)}-\int_0^1 x\cdot e^{\left(\int_0^x\left(-2\cdot(b\cdot t)+\frac{4\cdot\left(1-1\cdot e^{-1\cdot\left(b\cdot\left(t^2\right)\right)}\right)}{t}\right)dt\right)}dx$$

$$e^{2\gamma+2\ln(b)-b+2\,\mathrm{Ei}(1,b)}-\left(\int_0^1 x\,e^{\int_0^x\left(-2bt+\frac{4\left(1-e^{-bt^2}\right)}{t}\right)dt}\,dx\right)$$

```
> e^(int(-2*(b*t)+(10*(1-e^(-b*t^2)))/t, t=0..1))-int(x*e^(int(-2*(b*t)+(10*(1-1*e^(-1*(b*(t^2)))))/t, t=0..x))*e^(int(-2*(b*t)+(10*(1-1*e^(-1*(b*(t^2)))))/t, t=0..x)), x=0..1)
```

$$e^{\int_0^1\left(-2\,(b\cdot t)+\frac{10\cdot\left(1-e^{-b\cdot t^2}\right)}{t}\right)dt}-\int_0^1 x\cdot e^{\int_0^x\left(-2\cdot(b\cdot t)+\frac{10\cdot\left(1-1\cdot e^{-1\cdot(b\cdot(t^2))}\right)}{t}\right)dt}\cdot e^{\int_0^x\left(-2\cdot(b\cdot t)+\frac{10\cdot\left(1-1\cdot e^{-1\cdot(b\cdot(t^2))}\right)}{t}\right)dt}\,dx$$

$$e^{5\gamma+5\ln(b)-b+5\,\mathrm{Ei}(1,b)}-\left(\int_0^1 x\,e^{\int_0^x\left(-2bt+\frac{10\left(1-e^{-bt^2}\right)}{t}\right)dt}\,dx\right)$$

```
> fsolve( (1), b=11 )
```

$$fsolve\left(e^{5\gamma+5\ln(b)-b+5\,\mathrm{Ei}(1,b)}-\left(\int_0^1 x\,e^{\int_0^x\left(-2bt+\frac{10\left(1-e^{-bt^2}\right)}{t}\right)dt}\,dx\right),\ b=11\right)$$

```
> evalf[5]( (2) )
```

$$fsolve\left(e^{5\gamma+5\ln(b)-b+5\,\mathrm{Ei}(1,b)}-\left(\int_0^1 x\,e^{\int_0^x\left(-2bt+\frac{10\left(1-e^{-bt^2}\right)}{t}\right)dt}dx\right),b=11\right)$$

>

>

> $fsolve(\mathbf{(1)},b=5)$

$$-853.9990180$$

> $fsolve(\mathbf{(1)},b=10)$

2. Algebraic solution of tangential velocity of Multicellular vortex in Maple 13:

>

$$P := plot\left(\left[\frac{1}{r\cdot 4.371312758}\left(\int_0^r \left(\left(1+0.375\cdot r^2\right)^{\frac{1\cdot(-1)}{0.375}}\left(1+0.6\cdot r^2\right)^{\frac{1.1\cdot(-1)^2}{0.6}}\right)^{111.1532167} r\,dr\right)\right], r=0..3, y=0..1.0\right):$$

> $FileTools[Text][WriteString]("MaplePlot7t.txt", convert(P, string));$

6164

> $FileTools[Text][Close]("MaplePlot7t.txt");$

>

> PLOT(CURVES([[.4929004710e-3, .5637907464e-4], [.9858009420e-3, .1127586060e-3], [.1478701413e-2, .1691390509e-3], [.1971601884e-2, .2255208661e-3], [.2957402826e-2, .3382904344e-3], [.3943203768e-2, .4510709658e-3], [.5914805650e-2, .6766795387e-3], [.7886407535e-2, .9023758378e-3], [.1182961130e-1, .1354148723e-2], [.1577281507e-1, .1806624129e-2], [.2263473610e-1, .2596391255e-2], [.2949665713e-1, .3390243482e-2], [.4493055285e-1, .5197233141e-2], [.6046675445e-1, .7058276276e-2], [.7592911520e-1, .8967654213e-2], [.9026470294e-1, .1080277256e-1], [.1051083737, .1278341451e-1], [.1204597192, .1493465775e-1], [.1357618328, .1720165188e-1], [.1515019374, .1968261794e-1], [.1653658302, .2201189416e-1], [.1809732898, .2481865359e-1], [.1966448351, .2786048080e-1], [.2117472729, .3103240532e-1], [.2254617333, .3414288884e-1], [.2417695531, .3816164917e-1], [.2555844156, .4186969684e-1], [.2716543849, .4657525513e-1], [.2858790307, .5113136203e-1], [.3014857216, .5659985189e-1], [.3163469820, .6231243842e-1], [.3318531481, .6885404957e-1], [.3460926492, .7543584710e-1], [.3614518748, .8321147988e-1], [.3774057935, .9210091588e-1], [.3912937267, .1005730932], [.4062930750, .1105543146],

[.4217888694, .1218422708], [.4369484812, .1339165758], [.4516161850, .1466352553], [.4679021694, .1620247225], [.4825358507, .1770514582], [.4981604290, .1944062275], [.5123186192, .2113427836], [.5277972607, .2312112433], [.5423614562, .2512163848], [.5575852369, .2734921706], [.5724692652, .2966081204], [.5880514634, .3221915190], [.6030589723, .3481138477], [.6184063177, .3758431107], [.6336265794, .4044542003], [.6476124191, .4316066605], [.6636417698, .4635785218], [.6779786121, .4927785301], [.6932646762, .5243391540], [.7078953901, .5547531810], [.7241409176, .5884958670], [.7382083507, .6174607300], [.7541750131, .6497775002], [.7687268925, .6784688222], [.7846443617, .7087478801], [.7983784457, .7337374434], [.8140199642, .7606912684], [.8291288989, .7850031492], [.8442279632, .8074296818], [.8592714809, .8277721496], [.8737235918, .8453311037], [.8893467064, .8620480661], [.9042366674, .8757505285], [.9199076503, .8878154250], [.9340936634, .8966791628], [.9497718636, .9042615946], [.9647888474, .9094321215], [.9722790635, .9112795576], [.9797692794, .9126602106], [.9875928390, .9136216636], [.9954163987, .9141114311], [1.002622183, .9141629376], [1.009827967, .9138483420], [1.024587384, .9121329175], [1.040883534, .9087169361], [1.055638363, .9044096049], [1.070727940, .8989700709], [1.086073650, .8925212640], [1.100179345, .8859074897], [1.115215558, .8782608918], [1.130137315, .8701816927], [1.146098956, .8611202853], [1.160184413, .8528552759], [1.176436106, .8431016077], [1.191102007, .8341729954], [1.205613149, .8252791747], [1.221217288, .8157032035], [1.236884549, .8061227621], [1.251139437, .7974687450], [1.266277495, .7883709378], [1.281050760, .7796044211], [1.297065135, .7702442295], [1.310922021, .7622755275], [1.326837160, .7532811068], [1.341798226, .7449850387], [1.356614785, .7369239187], [1.371443131, .7290115971], [1.386567105, .7211010831], [1.402598264, .7128903295], [1.417297267, .7055171728], [1.431807071, .6983819709], [1.447317812, .6909084368], [1.462794787, .6836059451], [1.476686292, .6771799304], [1.493141781, .6697208787], [1.506910971, .6636036779], [1.523015585, .6565884645], [1.538385880, .6500295467], [1.552109722, .6442826717], [1.567543617, .6379396783], [1.583079820, .6316793678], [1.598542180, .6255695115], [1.612877767, .6200094730], [1.627721439, .6143555287], [1.643072784, .6086156330], [1.658374898, .6029998768], [1.674115002, .5973304755], [1.687978894, .5924244333], [1.703586355, .5869969308], [1.719257900, .5816462880], [1.734360337, .5765814422], [1.748074798, .5720578952], [1.764382619, .5667704856], [1.778197480, .5623672326], [1.794267450, .5573305125], [1.808492095, .5529468451], [1.824098787, .5482159224], [1.838960047, .5437856036], [1.854466213, .5392387267], [1.868705715, .5351297379], [1.884064940, .5307672672], [1.900018858, .5263105655], [1.913906791, .5224914841], [1.928906140, .5184285431], [1.944401935, .5142969577], [1.959561547, .5103182401], [1.974229251, .5065267873], [1.990515235, .5023824899], [2.005148915, .4987160767], [2.020773494, .4948600142], [2.034931685, .4914169881], [2.050410325, .4877072593], [2.064974522, .4842674761], [2.080198302, .4807233998], [2.095082330, .4773082115], [2.110664529, .4737844342], [2.125672037, .4704394575], [2.141019382, .4670672335], [2.156239644, .4637703433], [2.170225484, .4607816132], [2.186254834, .4574032196], [2.200591677, .4544232400], [2.215877742, .4512884357], [2.230508455, .4483282714], [2.246753983,

3. Algebraic solution of radial velocity of Multicellular vortex in Maple 13:

```
> P := plot([-1.0*r/(1+0.375*r^2)+0.9*r/(1+0.6*r^2), -1.0*r/(1+0.375*r^2)
  +0.8*r/(1+0.6*r^2), -1.0*r/(1+0.375*r^2)+0.7*r/(1+0.6*r^2), -1.0*r/(1+0.375*r^2)
  +0.6*r/(1+0.6*r^2)], r=0..8, y=0.1..-0.5):

> FileTools[Text][WriteString]("MaplePlot4t.txt", convert(P, string));

                                  31083

> FileTools[Text][Close]("MaplePlot4t.txt");

>

>
```

4. Algebraic solution of axial velocity of Multicellular vortex in Maple 13:

```
> P := plot([2/(1+0.375*r^2)^2-2.2/(1+0.6*r^2)^2, 2/(1+0.375*r^2)^2
  -2.26/(1+0.6*r^2)^2, 2/(1+0.375*r^2)^2-2.4/(1+0.6*r^2)^2], r=0..5,
  y=0.3..-0.3):

> FileTools[Text][WriteString]("MaplePlot3t.txt", convert(P, string));

                                  23497
```

> $FileTools[Text][Close](\text{"MaplePlot3t.txt"});$

>

5. Algebraic solution of pressure of Multicellular vortex in Maple 13:

>

$$P := plot\left(1.329769551 \left(\int_0^r \frac{1}{r^3} \left(0.05233307320 \left(\left(\int_0^r \left(\frac{\left(1+0.6r^2\right)^{1.833333333}}{\left(1+0.375r^2\right)^{2.666666667}} \right)^{111.1532167} r\,dr \right)^2 \right) dr \right), r = 0..6, y = 0..1.0 \right) :$$

> $FileTools[Text][WriteString](\text{"MaplePlot1t.txt"}, convert(P, string));$

5738

> $FileTools[Text][Close](\text{"MaplePlot1t.txt"});$

>

> PLOT(CURVES([[0., 0.], [.3154563015e-1, .8704525919e-5], [.5899331427e-1, .3086702520e-4], [.8986110573e-1, .7349170118e-4], [.1209335089, .1381390353e-3], [.1518582305, .2286295555e-3], [.1805294059, .3415456803e-3], [.2102167474, .4959916052e-3], [.2409194385, .7080305361e-3], [.2715236656, .9898718680e-3], [.3030038750, .1379372425e-2], [.3307316605, .1835707141e-2], [.3619465797, .2522748518e-2], [.3932896704, .3465551150e-2], [.4234945459, .4704660525e-2], [.4509234667, .6210403032e-2], [.4835391064, .8637821387e-2], [.5111688314, .1141107842e-1], [.5433087700, .1573190847e-1], [.5717580615, .2081658176e-1], [.6029714433, .2811735299e-1], [.6326939641, .3711881377e-1], [.6637062965, .4905054760e-1], [.6921852986, .6262170506e-1], [.7229037498, .8034978311e-1], [.7548115873, .1023384133], [.7825874536, .1244469958], [.8125861502, .1512553760], [.8435777391, .1817728037], [.8738969626, .2138625113], [.9032323704, .2464012789], [.9358043391, .2834713614], [.9650717017, .3169514403], [.9963208583, .3522329827], [1.024637239, .3833366791], [1.055594522, .4160218178], [1.084722913, .4452816828], [1.115170474, .4741760527], [1.144938531, .5007040514], [1.176102927, .5266684345], [1.206117945, .5499890254], [1.236812636, .5722196167], [1.267253159, .5927572712], [1.295224839, .6104004833], [1.327283540, .6292873917], [1.355957225, .6450683256], [1.386529353, .6608330521], [1.415790781, .6749783015], [1.448281836, .6896927489], [1.476416702, .7016581165], [1.508350027, .7144362678], [1.537453786, .7253955986], [1.569288724, .7366920894], [1.596756892, .7459010141], [1.628039929, .7558264478], [1.658257798, .7648854994], [1.688455927, .7734570888], [1.718542962, .7815517278], [1.747447184, .7889376729], [1.778693413, .7965205378], [1.808473335, .8033848194], [1.839815301, .8102521688], [1.868187328, .8161730656], [1.899543728, .8224106012], [1.929577695, .8281022106], [1.959538559, .8335212148], [1.990832798, .8389221815], [2.019655934, .8436761968], [2.049174768, .8483385205], [2.081767069, .8532576497], [2.111276727, .8575164312], [2.141455880, .8616910127], [2.172147301, .8657592544], [2.200358690, .8693495961], [2.230431116, .8730277627], [2.260274630, .8765337545], [2.292197913, .8801335234], [2.320368827, .8831875422], [2.352872214, .8865758470], [2.382204015, .8895152391], [2.411226298, .8923186743], [2.442434577, .8952224549], [2.473769099, .8980281156], [2.502278875, .9004898149], [2.532554990, .9030135425], [2.562101520, .9053906967], [2.594130270, .9078763617], [2.621844044, .9099540492], [2.653674320, .9122604935], [2.683596453, .9143542613], [2.713229571, .9163599090], [2.742886263, .9183024222], [2.773134211, .9202198137], [2.805196529, .9221848800], [2.834594535, .9239283675], [2.863614142, .9255970179], [2.894635624, .9273255706], [2.925589575, .9289958444], [2.953372585, .9304505096], [2.986283563, .9321214076], [3.013821943, .9334776783], [3.046031171, .9350175515], [3.076771761, .9364423374], [3.104219445, .9376788963], [3.135087235, .9390309196], [3.166159640, .9403521630], [3.197084361, .9416290634], [3.225755536, .9427802556], [3.255442879, .9439403410], [3.286145569, .9451071837], [3.316749796, .9462381852], [3.348230005, .9473693526], [3.375957790, .9483395873], [3.407172712, .9494036237], [3.438515801, .9504430052], [3.468720676, .9514181005], [3.496149597, .9522817737], [3.528765238, .9532826670], [3.556394961, .9541090990], [3.588534902, .9550465210], [3.616984191, .9558555339], [3.648197575, .9567214660], [3.677920095, .9575256299], [3.708932427, .9583441659], [3.737411430, .9590779607], [3.768129881, .9598508801], [3.800037718, .9606339616], [3.827813584, .9612997540], [3.857812282, .9620027362], [3.888803871, .9627119677], [3.919123095, .9633895941], [3.948458503, .9640304300], [3.981030471, .9647254373], [4.010297831, .9653355424], [4.041546989, .9659723843], [4.069863371, .9665368344], [4.100820651, .9671405972], [4.129949044, .9676963383], [4.160396605, .9682648150], [4.190164661, .9688086671], [4.221329059, .9693657473], [4.251344075, .9698907415], [4.282038766, .9704162469], [4.312479290, .9709263581], [4.340450970, .9713856665], [4.372509670, .9719012829], [4.401183356, .9723529431], [4.431755485, .9728248831], [4.461016912, .9732675324], [4.493507967, .9737489412], [4.521642832, .9741574493], [4.553576159, .9746119661], [4.582679916, .9750179598], [4.614514854, .9754532859], [4.641983023, .9758217232], [4.673266058, .9762334430], [4.703483928, .9766233689], [4.733682057, .9770056041], [4.763769094, .9773792268], [4.792673316, .9777315545], [4.823919543, .9781053288], [4.853699467, .9784548654], [4.885041431, .9788158537], [4.913413459, ..9850728632], [5.577781122, .9853067680], [5.607327651, .9855313931], [5.639356402, .9857709121], [5.667070173, .9859748939], [5.698900450, .9862055122], [5.728822583, .9864188096], [5.758455703,

.9866267785], [5.788112394, .9868317229], [5.818360342, .9870375333], [5.850422660, .9872522130], [5.879820667, .9874459752], [5.908840273, .9876344137], [5.939861756, .9878328049], [5.970815705, .9880276901], [6., .9882086780]],COLOUR(RGB,1.00000000,0.,0.)),AXESLABELS(r,y),VIEW(0. .. 6.,0. .. 1.0))

6. Algebraic solution of axial velocity of 4 cell vortex of in Maple 13:

> $\sum_{i=1}^{4} \frac{k_i (-1)^{i+1}}{\left(1 + b_i \cdot r^2\right)^2}$

$$\frac{k_i (-1)^2}{\left(1 + b_i r^2\right)^2} + \frac{k_i (-1)^3}{\left(1 + b_i r^2\right)^2} + \frac{k_i (-1)^4}{\left(1 + b_i r^2\right)^2} + \frac{k_i (-1)^5}{\left(1 + b_i r^2\right)^2}$$

> $\frac{1(-1)^2}{\left(1 + .1 \cdot r^2\right)^2} + \frac{2(-1)^3}{\left(1 + 0.2 r^2\right)^2} + \frac{2(-1)^4}{\left(1 + 0.785 r^2\right)^2} + \frac{2(-1)^5}{\left(1 + 5 r^2\right)^2}$

$$\frac{1}{\left(1 + 0.1 r^2\right)^2} - \frac{2}{\left(1 + 0.2 r^2\right)^2} + \frac{2}{\left(1 + 0.785 r^2\right)^2} - \frac{2}{\left(1 + 5 r^2\right)^2}$$

> > *smartplot*(**(1)**)

>

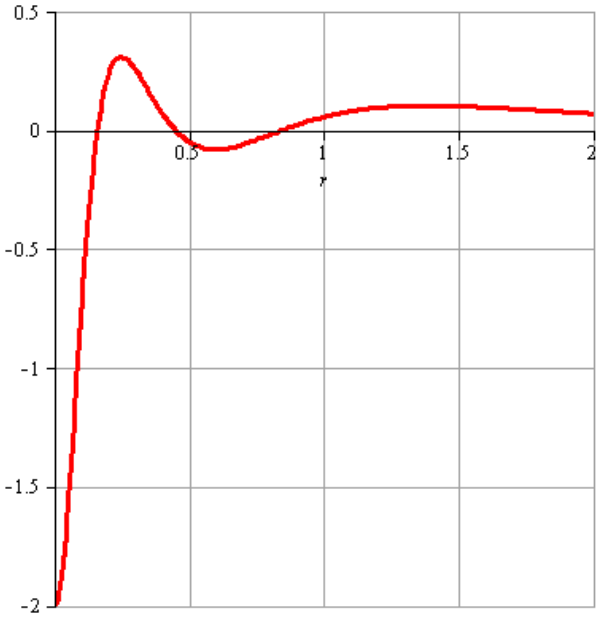

7. Algebraic solution of tangential velocity of 4 cell vortex of in Maple 13:

$$\int_0^2 \left(\frac{\left(1+0.2\,r^2\right)^{10.00000000}\left(1+5.0\,r^2\right)^{0.4000000000}}{\left(1+0.1\,r^2\right)^{10.00000000}\left(1+0.785\,r^2\right)^{2.547770701}} \right)^{116.54} r\,dr$$

> *evalf*[5](**(1)**)

$$6.4257\,10^5$$

>

> $$\frac{1}{r}\left(4.502922053\,10^{-7}\left(\int_0^r\left(\frac{\left(1+0.2\,r^2\right)^{10.00000000}\left(1+5.0\,r^2\right)^{0.4000000000}}{\left(1+0.1\,r^2\right)^{10.00000000}\left(1+0.785\,r^2\right)^{2.547770701}}\right)^{116.54} r\,dr\right)\right)$$

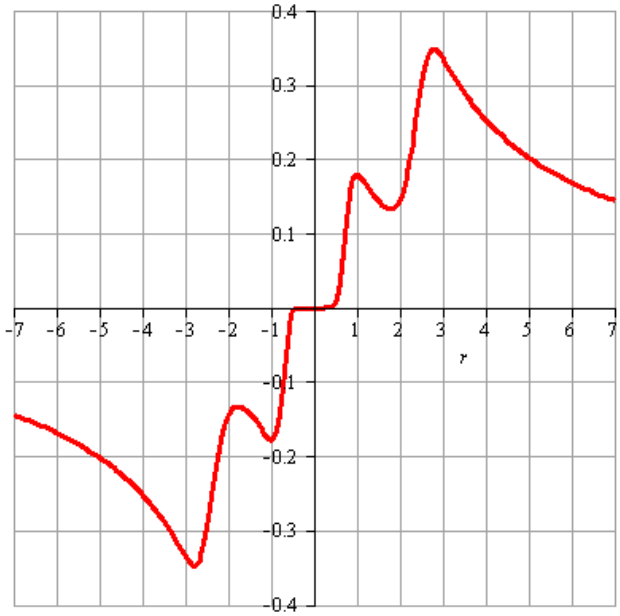

Appendix B

Code for extracted data point of tangential, radial, axial, velocity of Sullivan vortex model:

```
function [X,Y]=ReadMaplePlot1t(filename, Figure_Title)
% reads into matlab the data in a Maple plot structure
%
% in Maple 10 do
% > P:=plot(whatever multiple 2D plot); # this creates the plot structure. Plot in Maple with display(P);
% > FileTools[Text][WriteString]( "MaplePlot.txt", convert(P,string));
% > FileTools[Text][Close]( "MaplePlot.txt" );
%
% in Matlab do
% >> [Xdata, Ydata]=ReadMaplePlot('MaplePlot.txt','title, if you want a plot');

fileIn = char(textread(filename,'%s','whitespace','','bufsize',50000));
start=regexp({fileIn},'CURVES('); start=start{:}
ends=regexp({fileIn},',COLO'); ends=ends{:}
```

```
X=cell(length(start),1);
Y=cell(length(start),1);

for n=1:length(start)
eval(['d=' fileIn(start(n)+7:ends(n)-1) ';']);
X{n}=d(1:2:end);
Y{n}=d(2:2:end);
end


clc
clear all
close all
format long

% Data was saved in 'MaplePlot.txt' from Maple by using-
% FileTools[Text][WriteString]( "MaplePlot.txt", convert(P,string));
% FileTools[Text][Close]( "MaplePlot.txt" );


[X, Y]= ReadMaplePlot2t('MaplePlot2t.txt','Title');
```

```
figure(1);
if exist('Title')
plot(X{1},Y{1}); % Assuming 4 plots. Adjust accordingly
hold on
end

% To see variabales
% X1 = X{1}.' etc

X1 =X{1}.'
```

Code for extracted data point of tangential velocity of Multicellular vortex:

```
function [X,Y]=ReadMaplePlot7t(filename, Figure_Title)
% reads into matlab the data in a Maple plot structure
%
% in Maple 10 do
```

```
% > P:=plot(whatever multiple 2D plot); # this creates the plot structure. Plot in Maple with display(P);

% > FileTools[Text][WriteString]( "MaplePlot.txt", convert(P,string));

% > FileTools[Text][Close]( "MaplePlot.txt" );

%

% in Matlab do

% >> [Xdata, Ydata]=ReadMaplePlot('MaplePlot.txt','title, if you want a plot');


fileIn = char(textread(filename,'%s','whitespace','','bufsize',50000));

start=regexp({fileIn},'CURVES('); start=start{:}

ends=regexp({fileIn},',COLO'); ends=ends{:}


X=cell(length(start),1);

Y=cell(length(start),1);


for n=1:length(start)

eval(['d=' fileIn(start(n)+7:ends(n)-1) ';']);

X{n}=d(1:2:end);

Y{n}=d(2:2:end);

end


%
```

```
clc
clear all
close all
format long

% Data was saved in 'MaplePlot.txt' from Maple by using-
% FileTools[Text][WriteString]( "MaplePlot.txt", convert(P,string));
% FileTools[Text][Close]( "MaplePlot.txt" );



[X, Y]= ReadMaplePlot7t('MaplePlot7t.txt','Title');

figure(1);
if exist('Title')
plot(X{1},Y{1}); % Assuming 4 plots. Adjust accordingly
hold on
end

% To see variabales
% X1 = X{1}.' etc
```

Y1 =Y{1}.'

a= [

0

0.01

0.1633

0.2399

0.291

0.3932

0.4699

0.5721

0.6232

0.7509

0.8535

0.9013

0.9301

0.9539

0.9685

0.9834

0.9922

1.007

1.032

1.083

1.16

1.211

1.39

1.492

1.543

1.62

1.773

1.85

2.003

2.08

2.233

2.31

2.412

2.463

2.591

2.693

2.872

];

b = [

0

0.0011

0.02161

0.03772

0.05286

0.1018

0.1641

0.2961

0.385

0.6436

0.8199

0.8732

0.8943

0.9059

0.9104

0.9132

0.9139

0.9141

0.9108

0.8938

0.853

0.8219

0.7194

0.6702

0.6479

0.6173

```
0.564

0.5405

0.4991

0.4807

0.4478

0.4329

0.4146

0.406

0.386

0.3713

0.3481

];

plot(a,b,'r');
```

Code for extracted data point of radial velocity of Multicellular

```
function [X,Y]=ReadMaplePlot4t(filename, Figure_Title)

% reads into matlab the data in a Maple plot structure

%

% in Maple 10 do

% > P:=plot(whatever multiple 2D plot); # this creates the plot structure. Plot in Maple with display(P);

% > FileTools[Text][WriteString]( "MaplePlot.txt", convert(P,string));
```

```
% > FileTools[Text][Close]( "MaplePlot.txt" );
%
% in Matlab do
% >> [Xdata, Ydata]=ReadMaplePlot('MaplePlot.txt','title, if you want a plot');

fileIn = char(textread(filename,'%s','whitespace','','bufsize',50000));
start=regexp({fileIn},'CURVES('); start=start{:}
ends=regexp({fileIn},',COLO'); ends=ends{:}

X=cell(length(start),1);
Y=cell(length(start),1);

for n=1:length(start)
eval(['d=' fileIn(start(n)+7:ends(n)-1) ';']);
X{n}=d(1:2:end);
Y{n}=d(2:2:end);
end

%
clc
clear all
close all
format long
```

```
% Data was saved in 'MaplePlot.txt' from Maple by using-
% FileTools[Text][WriteString]( "MaplePlot.txt", convert(P,string));
% FileTools[Text][Close]( "MaplePlot.txt" );



[X, Y]= ReadMaplePlot4t('MaplePlot4t.txt','Title');


figure(1);
if exist('Title')
plot(X{1},Y{1},X{2},Y{2},X{3},Y{3},X{4},Y{4}); % Assuming 4 plots. Adjust accordingly
hold on
end


% To see variabales
% X1 = X{1}.' etc


Y4 =Y{4}.'


start =


     6       7770       15537       23295
```

```
ends =

        7739       15493       23251       31012
```

Code for extracted data point of axial velocity of Multicellular

```
function [X,Y]=ReadMaplePlot(filename, titulo)

% reads into matlab the data in a Maple plot structure

%

% in Maple 10 do

% > P:=plot(whatever multiple 2D plot); # this creates the plot structure. Plot in Maple with display(P);

% > FileTools[Text][WriteString]( "MaplePlot.txt", convert(P,string));

% > FileTools[Text][Close]( "MaplePlot.txt" );

%

% in Matlab do

% >> [Xdata, Ydata]=ReadMaplePlot('MaplePlot.txt','title, if you want a plot');


fileIn = char(textread(filename,'%s','whitespace','','bufsize',50000));

start=regexp({fileIn},'CURVES('); start=start{:};

ends=regexp({fileIn},',COLO'); ends=ends{:};
```

```
for n=1:length(start)
    eval(['d=' fileIn(start(n)+7:ends(n)-1) ';']);
    X(:,n)=d(1:2:end);
    Y(:,n)=d(2:2:end);
end

if exist('titulo')
    plot(X,Y);
    title(titulo);
end

clc
clear all
close all
format long
 % Data was saved in 'MaplePlot.txt' from Maple by using-
% FileTools[Text][WriteString]( "MaplePlot.txt", convert(P,string));
% FileTools[Text][Close]( "MaplePlot.txt" );
 [Xdata, Ydata]=ReadMaplePlot('MaplePlot.txt','Title');
 Xdata % To see Xdata
Ydata % To see Ydata
```